Acta Pharmaceutica Sinica B 2021;11(1):71−88

Chinese Pharmaceutical Association
Institute of Materia Medica, Chinese Academy of Medical Sciences

Acta Pharmaceutica Sinica B

www.elsevier.com/locate/apsb
www.sciencedirect.com

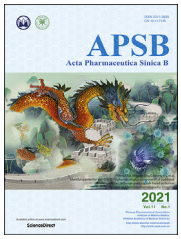

ORIGINAL ARTICLE

Activated PKB/GSK-3β synergizes with PKC-δ signaling in attenuating myocardial ischemia/reperfusion injury *via* potentiation of NRF2 activity: Therapeutic efficacy of dihydrotanshinone-I

Hao Zeng[†], Lingling Wang[†], Jiawei Zhang, Ting Pan, Yinghua Yu, Jingxia Lu, Ping Zhou, Hua Yang[*], Ping Li[*]

State Key Laboratory of Natural Medicines, School of Traditional Chinese Pharmacy, China Pharmaceutical University, Nanjing 210009, China

Received 29 July 2020; received in revised form 30 August 2020; accepted 31 August 2020

KEY WORDS

Dihydrotanshinone I;
NRF2;
Cytoplasmic/nuclear translocation;
PKC-δ;
PKB/GSK-3β/Fyn;
Phosphorylation;
Redox homeostasis;
Ischemia/reperfusion injury

Abstract Disrupted redox status primarily contributes to myocardial ischemia/reperfusion injury (MIRI). NRF2, the endogenous antioxidant regulator, might provide therapeutic benefits. Dihydrotanshinone-I (DT) is an active component in *Salvia miltiorrhiza* with NRF2 induction potency. This study seeks to validate functional links between NRF2 and cardioprotection of DT and to investigate the molecular mechanism particularly emphasizing on NRF2 cytoplasmic/nuclear translocation. DT potently induced NRF2 nuclear accumulation, ameliorating post-reperfusion injuries *via* redox alterations. Abrogated cardioprotection in NRF2-deficient mice and cardiomyocytes strongly supports NRF2-dependent cardioprotection of DT. Mechanistically, DT phosphorylated NRF2 at Ser40, rendering its nuclear-import by dissociating from KEAP1 and inhibiting degradation. Importantly, we identified PKC-δ-(Thr505) phosphorylation as primary upstream event triggering NRF2-(Ser40) phosphorylation. Knockdown of PKC-δ dramatically retained NRF2 in cytoplasm, convincing its pivotal role in mediating NRF2 nuclear-import. NRF2 activity was further enhanced by activated PKB/GSK-3β signaling *via* nuclear-export signal blockage independent of PKC-δ activation. By demonstrating independent modulation of PKC-δ and PKB/GSK-3β/Fyn signaling, we highlight the ability of DT to exploit both nuclear import and export regulation of NRF2 in treating reperfusion injury harboring redox homeostasis

*Corresponding authors. Tel./fax: +86 25 83271379.
E-mail addresses: liping2004@126.com (Ping Li), yanghua@cpu.edu.cn (Hua Yang).
[†]These authors made equal contributions to this work.
Peer review under responsibility of Chinese Pharmaceutical Association and Institute of Materia Medica, Chinese Academy of Medical Sciences.

https://doi.org/10.1016/j.apsb.2020.09.006

alterations. Coactivation of PKC and PKB phenocopied cardioprotection of DT *in vitro* and *in vivo*, further supporting the potential applicability of this rationale.

1. Introduction

Patients with myocardial infarction are urgent to re-open the occluded coronary artery through timely percutaneous coronary intervention[1], which limits the loss of cardiomyocytes from primary ischemia but meanwhile exacerbates secondary injury in reperfusion stage. This injury, termed myocardial ischemia/reperfusion injury (MIRI), contributes to morbidity and mortality in a worldwide range[2]. Myocardial ischemia/reperfusion involves multi-faceted pathogenic factors[3] which hampers the development of effective therapies. Amongst numerous targets implicated in MIRI, oxidative stress, initiating at the onset of reperfusion that triggers subsequent pathological process, is worthwhile intervention[4].

Nuclear factor erythroid 2-related factor 2 (NRF2) is the cardinal regulator of intrinsic antioxidant system, rendering itself a promising therapeutic target[5]. Under physiological condition, NRF2 is retained in cytoplasm, being connected to Kelch-like ECH-associated protein 1 (KEAP1) and constantly degraded by proteasome. Upon exposure to oxidative stress or other stimuli, NRF2 releases from KEAP1 and accumulated in nucleus to bind to antioxidant response elements (ARE), and cytoprotective gene expression is activated to confer cellular protection against oxidative stress[6]. The transcriptional regulatory activity of NRF2 is decided by its intranuclear accumulation, which is a multi-phase biological process under regulation of diversified signaling pathways. A first pivotal procedure for NRF2 nuclear accumulation is release from KEAP1[7], which allows NRF2 to be transported into nucleus by the intranuclear transporter, the importin family proteins[8]. Besides, the nuclear import process is also affected by other diverse nuclear import signals involving specific post-translational modifications[9−12]. On the other hand, NRF2 that has translocated to the nucleus also undergoes an export process primarily regulated by Fyn-dependent mechanism, which causes nuclear exclusion and inactivation of NRF2 signaling[13]. Considering the therapeutic significance of maintaining redox homeostasis in treating MIRI, regulating nuclear NRF2 accumulation by affecting nuclear import/export action might be a prospective strategy to limit reperfusion injury.

Salvia miltiorrhiza is a widely-used traditional Chinese medicine that has been applied to clinic for treating cardiovascular diseases in China for centuries[14]. In addition, modern clinical evaluations demonstrate that application of *S. miltiorrhiza* injection can provide clinical benefits to patients undergoing cardiopulmonary bypass surgery through attenuating oxidative stress[15]. Danshen was traditionally used by being boiled in water where the hydrophilic components primarily contributed to the cardioprotective effects. And now Danshen has been widely applied as varies forms of modern preparations, like tablets and capsules, which contain both hydrophilic phenolic acids as well as lipophilic tanshinones, and pharmacological research has identified both phenolic acids and tanshinones as effective cardioprotective components of Danshen[16−20]. Dihydrotanshinone I (DT) is one of the principal tanshinone derivatives in *S. miltiorrhiza* with reported healthy benefits including cardioprotection and skin protection[21,22]. A previous study has reported that DT attenuated myocardial reperfusion injury *via* inhibition of arachidonic acid ω-hydroxylase[23]. Since upregulation of arachidonic acid ω-hydroxylase can be triggered by disrupted redox status[24] and meanwhile get restricted upon NRF2 activation[25,26], whether these beneficial effects of DT are mediated *via* modulation of NRF2 signaling has not been solidly elucidated yet. In addition, DT activates NRF2 with reducing ROS production in skin cells, and it is shown to inhibit NRF2 degradation and thus attenuate lung injury by suppressing inflammation[27,28]. Although modification of NRF2 degradation is proposed to be an important contributor to DT-induced NRF2 activation, the upstream biological events responsible for this phenomenon still remain unclear. Moreover, whether DT can modulate NRF2 signaling by directly affecting the nuclear/cytoplasmic translocation process has rarely been investigated. For these reasons, in this study, we aim at clarifying the links between NRF2-induction activity and cardioprotection of DT against MIRI, and further seek to investigate the regulatory mechanism of NRF2 signaling by focusing on the cytoplasmic/nuclear translocation process.

2. Materials and methods

2.1. Chemical and reagents

DT was purchased from Chengdu MUST biotechnology (Chengdu, China) and the purity was determined using HPLC ($\geq$98%). Specific protein kinase B (PKB) inhibitor MK-2206 (HY-10358), protein kinase C (PKC) inhibitor Go-6983 (HY-13689), PKC activator phorbol 12-myristate 13-acetate (PMA, HY-18739), PKB activator SC79 (HY-18749), protein synthesis inhibitor cycloheximide (CHX, HY-12320), proteasome inhibitor MG-132 (HY-13259) and nuclear import inhibitor SN50 (HY-P0151) were purchased from MedChemExpress (Princeton, NJ, USA). Nuclear export inhibitor leptomycin B (LMB, S1726) was purchased from Beyotime biotechnology (Shanghai, China). Specific inhibitor for GSK-3β phosphorylation differentiation-inducing factor 3 (DIF-3, D0567) and nuclear dye 4′,6-diamidino-2-phenylindole (DAPI, D8417) were purchased from Sigma−Aldrich (St. Louis, MO, USA). CELLROX fluorescent dye (C10444), nuclear and cytoplasmic extraction reagents (78833) and MitoTracker® Red CMXRos (M7512) were purchased from Thermo Fischer Scientific (Waltham, MA, USA). Primary antibodies against NRF2 (16396-1-AP) and importin-α5 (18137-1-AP) were purchased from Proteintech (Rosemont, PA, USA). PKB (4691), ubiquitin (3933), normal rabbit IgG (2729), lamin-B1 (12586), phosphorylated-GSK-3β (Ser9, 14630), GSK-3β (12456), PKC-α (2056), PKC-ε (2683), PKC-δ (2058), phosphorylated-PKC-δ (Thr505, 9374), phosphorylated-PKB

(Ser473, 4060), Fyn (4023) and importin-β1 (51186) were purchased from Cell Signaling Technology (Danvers, MA, USA). PKC-η (ab179524), phosphorylated-NRF2 (Ser40, ab76026), 8-hydroxy-2′-deoxyguanosine (8-OHDG, ab48508), α-actinin (ab68167) and GAPDH were obtained from Abcam (Cambridge, UK). KEAP1 antibody (MA5-17106) was purchased from Thermo Fischer Scientific. IR dye-conjugated secondary antibodies were purchased from LI-COR Biosciences (Lincoln, NE, USA).

2.2. Drug preparation and administration

For animal experiments, DT was freshly prepared in 0.5% sodium carboxymethylcellulose aqueous solution, and drug was administered by gavage 3 h before ischemia/reperfusion operation. For cellular experiments, DT was prepared as stock solution in DMSO at the concentration of 5 mmol/L and stored at −80 °C, and DT was diluted to working concentration (0.1, 1, and 5 μmol/L) in culture media and applied to cardiomyocytes for 6 h before hypoxia/reoxygenation treatment.

2.3. Animal experiments and grouping

Wild type male C57BL/6 mice and *Nrf2*-knockout mice constructed on a C57BL/6 background were purchased from Model Animal Research Center of Nanjing University (Nanjing, China). All animals were maintained with 12 h of light/12 h of dark cycle, 25 °C and 55% of relative humidity, and free access to food and water. All experimental protocols conducted on the mice were approved by the Institutional Animal Care and Use Committee at China Pharmaceutical University (Nanjing, China) in accordance with the standards established by the Laboratory Animal Welfare and Ethics Committee of China. After acclimating to the housing environment for 7 days, mice were randomly assigned to sham, I/R and respective medication groups (n = 5 to 6 mice for each experimental group as indicated).

2.4. Mouse model of myocardial ischemia/reperfusion

Mice were subjected to ischemia/reperfusion as previously described[29]. Briefly, mice were anesthetized with pentobarbital (50 mg/kg body weight, intraperitoneal injection), and the left anterior descending artery (LAD) was ligated with 6-0 silk. Ischemia was confirmed by an immediate color change of the myocardium supplied by the vessel from bright red to pale and an ST-segment elevation shown in electrocardiogram. Following 30 min of LAD occlusion, the ligature was released, and the mice were allowed to recover. Injury indicators were determined at different time points after reperfusion.

For preliminary evaluation of therapeutic efficacy of DT, ischemia/reperfusion experiments were conducted on wild type male C57BL/6 mice (aged 8−10 weeks). For validation of the NRF2-dependency of DT's cardioprotection, experiments were parallelly carried out on male wildtype and *Nrf2*-KO animals (aged 8−10 weeks) to compare the therapeutic efficacy.

2.5. Evaluation of myocardial infarct size

Myocardial infarct size was evaluated by 2,3,5-triphenyl tetrazolium chloride (TTC) staining as previously described[30]. Briefly, at the end of the 24 h reperfusion, the heart was excised and then quickly frozen at −80 °C for 6 min. Thereafter, the heart was cut into 4 to 5 pieces equably below the ligation position of the heart, followed by incubation for 10 min at 37 °C in a phosphate-buffered 1% TTC solution to determine infarcted myocardium. The infarcted tissues remained pale, whereas normal tissues were stained red. The pictures were captured with a digital camera (Canon, Tokyo, Japan) and infarct size was analyzed by using Image Pro Plus (IPP) 6.0 software (Media Cybernetics, Bethesda, MD, USA).

2.6. Echocardiography

Echocardiography was performed at 2 weeks after reperfusion with the Vevo 2100 imaging system (Visual Sonics Inc., Toronto, Ontario, Canada) and a 30-MHz probe was applied to measure left ventricular (LV) end-diastolic diameter (LVEDD), LV end-systolic diameters (LVESD), anterior wall diastolic thickness (AWDT), anterior wall systolic thickness (AWST), posterior wall diastolic thickness (LVPWDT), and posterior wall systolic thickness (PWST) at M-Mode. Fractional shortening (FS), ejection fraction (EF), and left ventricular mass (LV mass) were calculated. The investigator performing and reading the echocardiogram was blinded to the treatment allocation.

2.7. 8-OHDG staining

Nuclear staining of 8-OHDG was performed as previously described[31]. Heart cross-sections were placed in Coplin jars with 0.05% citraconic anhydride solution, pH 7.4 for 1 h at 98 °C and then incubated overnight at 4 °C with the first antibody, followed by the appropriate secondary antibody at 37 °C for 40 min. Immunofluorescence studies were performed by applying monoclonal antibody against 8-OHDG to detect hydroxyl radical-induced DNA oxidation as a sensitive and stable index of oxidative stress in cells. Monoclonal antibody against α-actinin was used to detect cardiomyocytes. Anti-rabbit IgG (H+L), F(ab′)2 fragment (Alexa Fluor 488 conjugate) and anti-mouse IgG (H+L), F(ab′)2 fragment (Alexa Fluor 555 conjugate) (Cell Signaling Technology) were used as secondary antibodies. Sections were counterstained with DAPI and mounted with fluorescent mounting medium (Vectashield, Vector Laboratories, Jon Burlingame, CA, USA) for fluorescence microscopic analysis using a DeltaVision Ultra microscopic imaging system (GE Life Science, Boston, MA, USA). All sections were evaluated with IPP 6.0 software.

2.8. Determination of cross-sectional area of cardiomyocytes

Determination of cross-sectional area of cardiomyocytes in LV was performed as described previously[32]. 5-μm thick heart cross-sections were counter-stained with wheat germ agglutinin (WGA, Thermo Fischer Scientific) and DAPI. Fluorescent images were captured with a DeltaVision Ultra microscopic imaging system (GE Life Science).

2.9. Cell culture experiments and grouping

HL-1 mouse cardiac cells were purchased from the Jennio Biotech Co., Ltd. (Guangzhou, China). Cells were cultured in 1× Dulbecco's modified Eagle's medium (DMEM; 10569044, GIBCO,

Thermo Fischer Scientific) supplemented with 10% fetal bovine serum (FBS; 10099141, GIBCO, Thermo Fischer Scientific) and antibiotics (100 unit/mL penicillin and 100 μg/mL streptomycin, 15140-122, GIBCO, Thermo Fischer Scientific) at 37 °C in a humidified incubator containing 5% CO_2 and 95% atmosphere. The medium was changed approximately every 24 h. Once the HL-1 cells reached confluence, cell cultures were split 1 to 3, and this was designated as a passage. All experiments were performed using cells between passages 5 and 15. New cultures were regularly re-established from frozen stocks every 2 months. For cell experiments, cells were seeded in petri-dishes or multi-well plates and cultured to reach 90% confluency, and then the cells were serum-starved overnight or for 12 h before subsequent treatment.

For cell culture experiments, immunoprecipitation experiments were conducted for 3 times, and other experiments were repeatedly performed for 5 times. All multi-well and imaging assays [including cell viability, lactate dehydrogenase (LDH) leakage, ROS content and immunofluorescence experiments] were triplicated for each separate experiment, and Western blot experiments were repeatedly performed with 5 batches of different samples without duplicates.

2.10. Hypoxia/reoxygenation model

Hypoxia/reoxygenation experiments were performed as previously described with minor modifications[33]. HL-1 cells were seeded at the density of 1.0×10^4 cells/well in a 96-well plate and cultured to reach 90% confluency. After serum-starved overnight, cells were pretreated with vehicle or indicated drugs for 6 h. For simulated hypoxia, culture medium was replaced with 100 μL glucose-free DMEM (323381, Sigma−Aldrich) and cells were incubated in a humidified tri-gas incubator equilibrated with 94% N_2, 5% CO_2 and 1% O_2 for 8 h. Reoxygenation was initiated by buffer exchange to 100 μL normal glucose culture medium and incubation in 95% atmosphere and 5% CO_2 for another 3 h.

2.11. Cell viability assays

Cell viability was determined by a colorimetric procedure with the cell counting kit-8 (CCK-8, Dojindo Laboratories, Kumamoto, Japan) according to manufacturer's instructions. Cells were seeded at a density of 1.0×10^4 cells/well in a 96-well plate. After addition of CCK-8 working solution, cells were incubated at 37 °C for 3 h, and cell viability was determined by measuring the absorbance at 450 nm on a POLARstar Omega microplate reader (BMG Labtech, Offenburg, Germany).

2.12. Determination of LDH leakage

LDH leakage was determined by a colorimetric procedure with the cytotoxicity LDH assay kit (Dojindo Laboratories) according to manufacturer's instructions. Cells were seeded at a density of 1.0×10^4 cells/well in a 96-well plate. After cells were pretreated with indicated stimulations, 30 μL culture medium per well was collected and 100 μL of LDH assay buffer was added to initiate the colorimetric reaction, and the mixture was incubated at 37 °C for 30 min and LDH activity was determined by measuring the absorbance at 490 nm on a POLARstar Omega microplate reader (BMG Labtech).

2.13. Measurement of malondialdehyde (MDA)

MDA was measured by a colorimetric method with the MDA assay kit (Beyotime biotechnology) according to manufacturer's instructions. Cells were seeded at a density of 2.0×10^5 cells/well in a 6-well plate. After cells were pretreated with indicated stimulations, 100 μL lysis buffer per well was added and lysate was collected and centrifuged at 4 °C, 12,000×g for 10 min. Supernatant was collected and used for subsequent measurement. The protein content was determined by BCA method using a Pierce BCA protein assay kit (23225, Pierce, Thermo Fischer Scientific). For the measurement of MDA, TBA buffer was added to sample to start up the colorimetric reaction, the solution was incubated at 100 °C for 10 min and MDA concentration was determined by measuring the absorbance at 532 nm, results were adjusted with BCA value and expressed as μmol/g protein.

2.14. Determination of intracellular ROS content

Intracellular ROS content was determined with a green fluorescent dye CellROX following manufacturer's instructions. Cells were stained with CellROX reagent at a final concentration of 5 μmol/L at 37 °C for 30 min. After washing, fluorescent images were captured by a DeltaVision Ultra microscopic imaging system (GE Life Science), and fluorescent intensity was calculated with IPP 6.0 software.

2.15. Immunofluorescence

Cells were fixed with 3.7% paraformaldehyde diluted in warm PBS for 15 min, followed by permeabilizing and blocking in blocking buffer (5% normal goat serum (005-000-121, Jackson ImmunoResearch Inc., Bar Harbor, ME, USA) and 0.3% Triton-X-100 in PBS) for 60 min. Immunostaining were performed by incubation with specific primary antibody at 4 °C overnight. Anti-rabbit IgG (H+L), F(ab′)2 fragment (Alexa Fluor 488 conjugate) or anti-mouse IgG (H+L), F(ab′)2 fragment (Alexa Fluor® 555 conjugate, Cell Signaling Technology) were used as secondary antibodies. Cells were counterstained with DAPI and mounted with Vectashield fluorescent mounting medium (Vector Laboratories) for fluorescent microscopic analysis using a DeltaVision OMX or DeltaVision Ultra microscopic imaging system (GE Life Science). For samples counterstained with Mitotracker, cells were first stained with MitoTracker® Red CMXRos (200 nmol/L), followed by standard immunofluorescent procedures.

2.16. RNA interference

For RNAi experiments, siRNA targeting *Nrf2* and scrambled siRNA (Genepharma, Shanghai, China) were used (siRNA sequences were listed in Table 1). For a single well of a 6-well plate, 100 pmol siRNA and 10 μL Xfect RNA transfection polymer (631450, Takara, Kyoto, Japan) were added to 200 μL Xfect reaction buffer, mixed thoroughly and placed at room temperature for 10 min to generate a transfection mixture. For transfection, culture medium was replaced with antibiotic-free DMEM and transfection mixture was added. The plate was incubated at 37 °C for 4 h and transfection complexes were removed and replaced

Table 1 Nucleotide sequences of siRNA.

Species	Name	Sequence (5′−3′)
Mus musculus	*Nrf2* siRNA	Sense: CGAGAAGUGUUUGACUUUATT Antisense: UAAAGUCAAACACUUCUCGTT
Mus musculus	*Pkc-α* siRNA	Sense: CCAUCAAGAUCCUGAAGAATT Antisense: UUCUUCAGGAUCUUGAUGGTT
Mus musculus	*Pkc-δ* siRNA	Sense: CCAAGGACAUCAUGGAGAATT Antisense: UUCUCCAUGAUGUCCUUGGTT
Mus musculus	*Pkc-η* siRNA	Sense: GGAAAGUGUUUGUGGUAAUTT Antisense: AUUACCACAAACACUUUCCTT
Mus musculus	*Pkc-ε* siRNA	Sense: UCAUCAAGGUGUUGGGCAATT Antisense: UUGCCCAACACCUUGAUGATT
Mus musculus	Scrambled siRNA	Sense: UUCUCCGAACGUGUCACGUTT Antisense: ACGUGACACGUUCGGAGAATT

with fresh media. Analysis of knockdown efficiency and other experiments were conducted 24 h post-transfection.

2.17. Plasmid transfection

For plasmid transfection, plasmid overexpressing *Nrf2* (pcDNA, VectorBuilder, Guangzhou, China) was used. For a single well of a 6-well plate, 2.5 μg plasmid and 0.75 μL Xfect RNA Transfection Polymer (631317, Takara) were added to 100 μL Xfect reaction buffer, mixed thoroughly and placed at room temperature for 10 min to generate a transfection mixture. For transfection, culture medium was replaced with antibiotic-free DMEM and transfection mixture was added. The plate was incubated at 37 °C for 4 h and transfection complexes were removed and replaced with fresh media.

2.18. Adeno-associated virus serotype 9 (AAV9)-based cardiac-specific knockdown of Nrf2

For cardiac-specific knockdown of *Nrf2* in mice, recombinant adeno-associated virus (serotype 9) vectors carrying mouse *Nrf2* with a *c-Tnt* promoter (AAV9-*Nrf2*, Hanbio Inc., Shanghai, China) were used[34]. In brief, mice were injected with 100 μL of AAV9-*Nrf2* virus suspension (virus titer$>10^{12}$ vg/mL) blend with 100 μL normal saline. Control mice were parallelly injected with equal amount of AAV9-control. After validation of cardiac *Nrf2*-knockdown efficiency 3 weeks after AAV9 injection by using q-PCR and Western blot method, mice were randomly divided into different groups and subjected to subsequent I/R experiments.

2.19. Ubiquitination analysis

36 h after transfection with plasmids overexpressing *Nrf2*, cells were pretreated with vehicle or proteasome inhibitor MG-132 (5 μmol/L) for 6 h, followed stimulation with vehicle or DT for another 6 h. Immunoprecipitation was conducted using a Pierce™ Classic Magnetic IP/Co-IP Kit (88804, Thermo Fischer Scientific). Whole cell lysate was collected and incubated with 1 μg of *Nrf2* or IgG primary antibody at 4 °C on a rocker overnight. Twenty microliters of resuspended protein A/G magnetic beads were added to the samples, followed by incubation at 4 °C for 4 h. Immunoprecipitate was collected and the sediments were washed three times in lysis buffer, resuspended in 80 μL of elution buffer at room temperature for 5 min. The eluted proteins were analyzed by standard Western blot procedures with an anti-ubiquitin antibody.

2.20. Isolation of cytoplasmic/nuclear protein

Cytoplasmic and nuclear protein of cardiac tissues or cultured cells was isolated with NE-PER nuclear and cytoplasmic extraction reagents (Thermo Fischer Scientific) according to manufacturer's instructions. For heart samples, 30 mg tissue per heart was used and homogenate was prepared by using an oscillating homogenizer. For culture cells, 1×10^7 cells per sample were used.

2.21. Western blot

Protein samples were resolved on polyacrylamide gels and transferred to 0.45 μm nitrocellulose filter membranes. Membranes were blocked with nonfat milk (5% in Tris-buffered saline, TBS) for 0.5 h at room temperature, and then with primary antibody in TBS supplemented with 3% bovine serum album (BSA) overnight at 4 °C. Membranes were washed with TBST (3×10 min), then incubated with the appropriate secondary antibody in TBS at room temperature for 2 h and washed again. Protein quantification was performed on an odyssey Sa Imaging System (LI-COR Biosciences).

2.22. RNA isolation and quantitative-PCR (q-PCR)

Total RNA from tissue or cell samples was isolated using total RNA extraction reagent (R401-1, Vazyme Biotech, Nanjing, China) and reversed transcribed using a HiScript II reverse transcription system (R223-1, Vazyme Biotech) according to the manufacturers' instructions. q-PCR experiment was performed in a 20 μL reaction system, which contains 10 μL AceQ qPCR SYBR green master mix (Q121-1, Vazyme Biotech), 7 μL H_2O, 2 μL cDNA, and 1 μL primer, using the LightCycler480 q-PCR system (Roche Molecular Systems, Inc., Basel, Switzerland). 18S was used as internal reference and relative gene expression was expressed as the percentage of expression level in control group. The primer sequences for *Nrf2*, *Ho-1*, *Nqo-1*, *Gclc* and 18s were listed in Table 2.

2.23. Randomization and blinding

In mice I/R experiments, mice were randomly assigned to sham, model and drug treatment conditions. Then, cyto-biology and

Table 2 Nucleotide sequences of q-PCR primers.

Species	Gene of interest	Sequence (5′−3′)
Mus musculus	*Nrf2*	Sense: CGAGATATACGCAGGAGAGGTAAGA Antisense: GCTCGACAATGTTCTCCAGCTT
Mus musculus	*Ho-1*	Sense: TGACAGAAGAGGCTAAGACCG Antisense: AGTGAGGACCCACTGGAGGA
Mus musculus	*Nqo-1*	Sense: CGCCTGAGCCCAGATATTGT Antisense: GGAAAGGACCGTTGTCGTAC
Mus musculus	*Gclc*	Sense: CAGTCAAGGACCGGCACAAG Antisense: CAAGAACATCGCCTCCATTCAG
Mus musculus	*18s*	Sense: CGGCTACCACATCCAAGGAA Antisense: GCTGGAATTACCGCGGCT

molecular biology detection was carried out in blind fashion. Data statistics were also run in blind fashion.

2.24. Statistical analysis

All data are expressed as mean ± standard deviation (SD) unless otherwise noted. Significance between two groups was performed by Student's two-tailed *t*-test with GraphPad Prism 6.01 (GraphPad Software, La Jolla, CA, USA). In other cases, significance across more than two groups was done in Prism with one-way ANOVA. $P < 0.05$ was considered significant for all tests.

3. Results

3.1. DT induces NRF2 activation and ameliorates myocardial ischemia/reperfusion and hypoxia/reoxygenation injury with maintained redox homeostasis

Firstly, the protective effects of DT (see chemical structure in Fig. 1A) against MIRI were investigated in mouse model. DT was administered to C57BL/6 mice (5 mg/kg body weight) by gavage 3 h before ischemia/reperfusion (I/R) operation following examination of injury indicators at different time points. Myocardial infarct size was determined using TTC staining at 24 h after the operation. As a result, infarct size increased to 34% after I/R insult and was restored to 23% by DT pretreatment (Fig. 1B). Cardiac functions were determined 2 weeks after I/R operation: I/R significantly impaired cardiac functions, indicated by marked decrease in EF (from 64% to 45%) and FS (from 35% to 22%), and were preserved to 53% and 27% by DT (Fig. 1C). I/R-induced pathological ventricular hypertrophy, indicated by increased cross-sectional area of cardiomyocytes, was also blunted by DT (Fig. 1D). For further evaluation of oxidative injury, nuclear staining of 8-OHDG as a signature of free radical formation was performed in LV. As a result, nuclear 8-OHDG intensity markedly increased after I/R and was also relieved by DT treatment (Fig. 1E). To elucidate the possible protective mechanism of DT, we examined nuclear protein level of NRF2, the key transcriptional factors regulating antioxidant system. As a result, nuclear NRF2 content was slightly elevated (2.3-fold) after I/R insult, probably as an adaptive response to I/R-induced oxidative injury, and DT pretreatment augmented nuclear NRF2 to a much higher level (5.8-fold, Fig. 1F).

To further examine cellular cardioprotection of DT, an *in vitro* H/R model on HL-1 mouse cardiomyocytes was applied. Notably, pretreatment of DT potently ameliorated H/R-induced cell viability reduction (Fig. 1G). LDH leakage is a pivotal indicator of cytomembrane integrity. We show that H/R substantially increased LDH leakage in the supernatant (5.6-fold of control group), and such increase could be significantly ameliorated by DT (Fig. 1H). The content of lipid peroxidation intracellular product MDA, a direct index of oxidative stress, increased from 2.0 to 5.8 μmol/g protein in H/R-exposed cells and was dose-dependently decreased by DT, reaching a minimum value of 2.9 μmol/g protein at 5 μmol/L (Fig. 1I). Therefore, DT at 5 μmol/L was employed in subsequent cell experiments unless otherwise noted. In addition, intracellular ROS level, indicated by CELLROX intensity, H/R challenge was shown to elevate intracellular ROS level to about 2.1-fold of control cells and DT was shown to restore it to 1.2-fold (Fig. 1J). Furthermore, nuclear NRF2 level was shown to elevate dose-dependently by DT pretreatment, which is consistent with the *in vivo* results (Fig. 1K).

Above results collectively support that DT pretreatment can potently ameliorate MIRI with improved redox homeostasis, and significant induction of NRF2 is associated.

3.2. Cardioprotective effects of DT is dependent on NRF2-mediated antioxidative response

Being illustrated that DT activated NRF2 signaling, reduced myocardial infarct size and finally preserved cardiac functions after I/R, we wondered whether DT-provided cardioprotection were dependent on NRF2 antioxidative response *in vivo*. Therefore, global *Nrf2*-knockout (*Nrf2*-KO) mice were constructed and animal experiments were parallelly conducted on wildtype and *Nrf2*-KO animals to compare the therapeutic efficacy. *Nrf2* knockout was validated in cardiac tissues by Western blot and q-PCR experiments (Fig. 2A and B). Accordingly, expression of NRF2 downstream genes *Ho-1*, *Nqo-1* and *Gclc* was extensively downregulated (*Ho-1*: 47%, *Nqo-1*: 23%, *Gclc*: 33%, compared to WT mice) in *Nrf2*-KO mice (Fig. 2C−E). Despite that no significant differences in EF and FS existed between healthy WT mice and *Nrf2*-KO mice, *Nrf2*-KO mice exhibited exacerbated infarct size and cardiac functions compared to WT mice after I/R, probably as a result of deficiency in antioxidative system. Importantly, DT-provided cardioprotective effects were blunted in *Nrf2*-KO mice, represented by comparable infarct size, EF, FS and LV mass in DT and vehicle-treated *Nrf2*-KO mice (Fig. 2F and G). Consistently, DT failed to significantly improve the injury indicators examined by WGA and 8-OHDG staining (Fig. 2H and I) in *Nrf2*-KO mice.

To further examine the role of NRF2 for DT-provided protection *in vitro*, specific siRNA targeting *Nrf2* was applied in HL-1

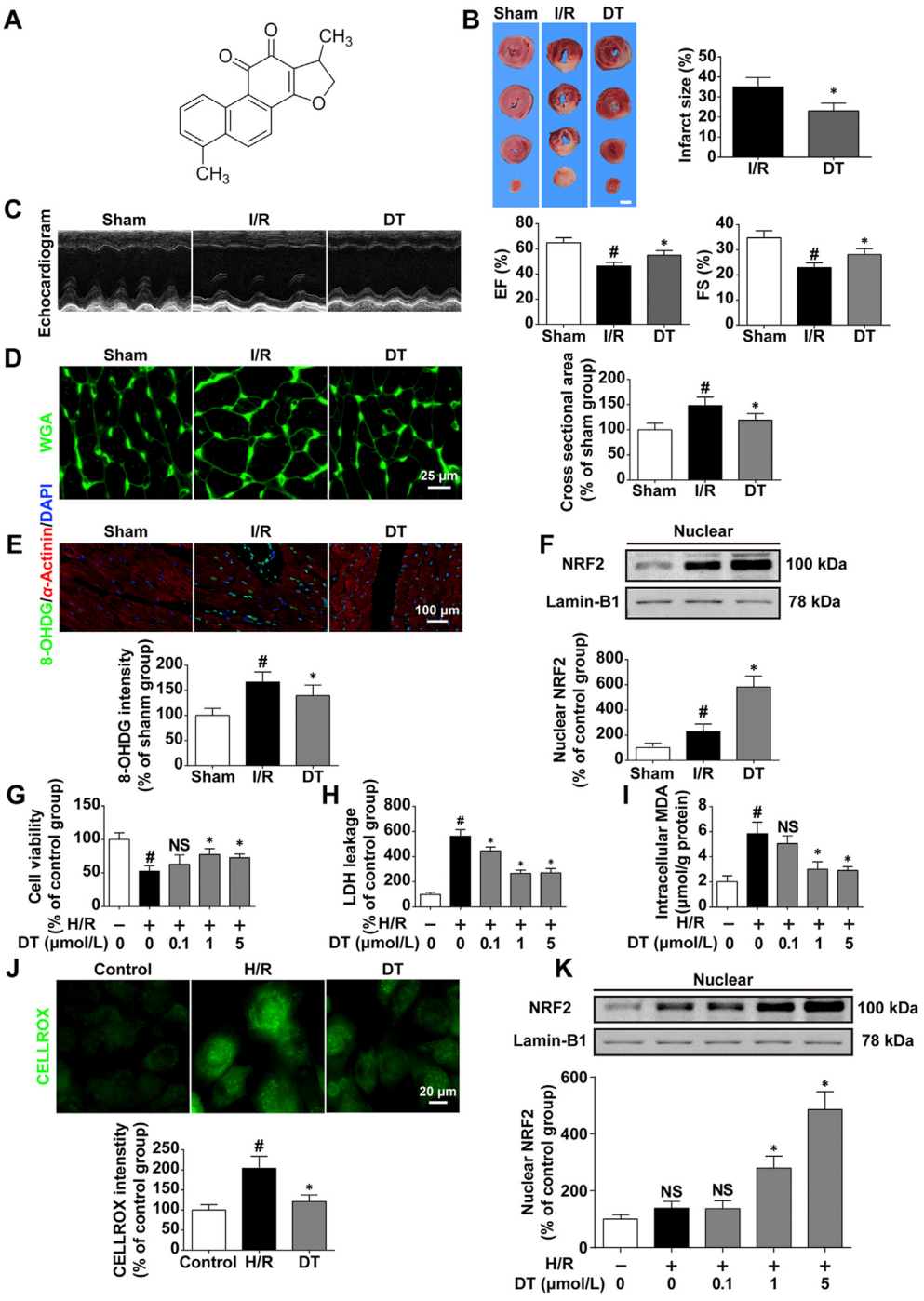

Figure 1 DT induces NRF2 activation and ameliorates myocardial ischemia/reperfusion and hypoxia/reoxygenation injury with maintained redox homeostasis. (A) Chemical structure of dihydrotanshinone I. (B) Representative images and calculated infarct size of the myocardium, scale bar = 2 mm (n = 5). (C) Echocardiogram of LV and the calculated EF and FS (n = 6). (D) Representative images of WGA-stained LV sections and the calculated cross-sectional area of cardiomyocytes, scale bar = 25 μm (n = 6). (E) Representative images of 8-OHDG/α-actinin/DAPI-stained LV sections and the calculated nuclear 8-OHDG intensity, scale bar = 100 μm (n = 6). (F) Nuclear protein level of NRF2 in the myocardium of sham, I/R and DT-treated mice (n = 5). (G)–(I) Cell viability, extracellular LDH leakage and intracellular MDA content of cardiomyocytes (n = 5). (J) Representative images of CELLROX-stained cardiomyocytes, scale bar = 20 μm (n = 5). (K) Nuclear protein level of NRF2 in control, H/R and DT-treated cardiomyocytes (n = 5). Data are expressed as mean ± SD, $^{\#}P < 0.05$ *versus* sham or control group; $^{*}P < 0.05$ *versus* I/R or H/R group.

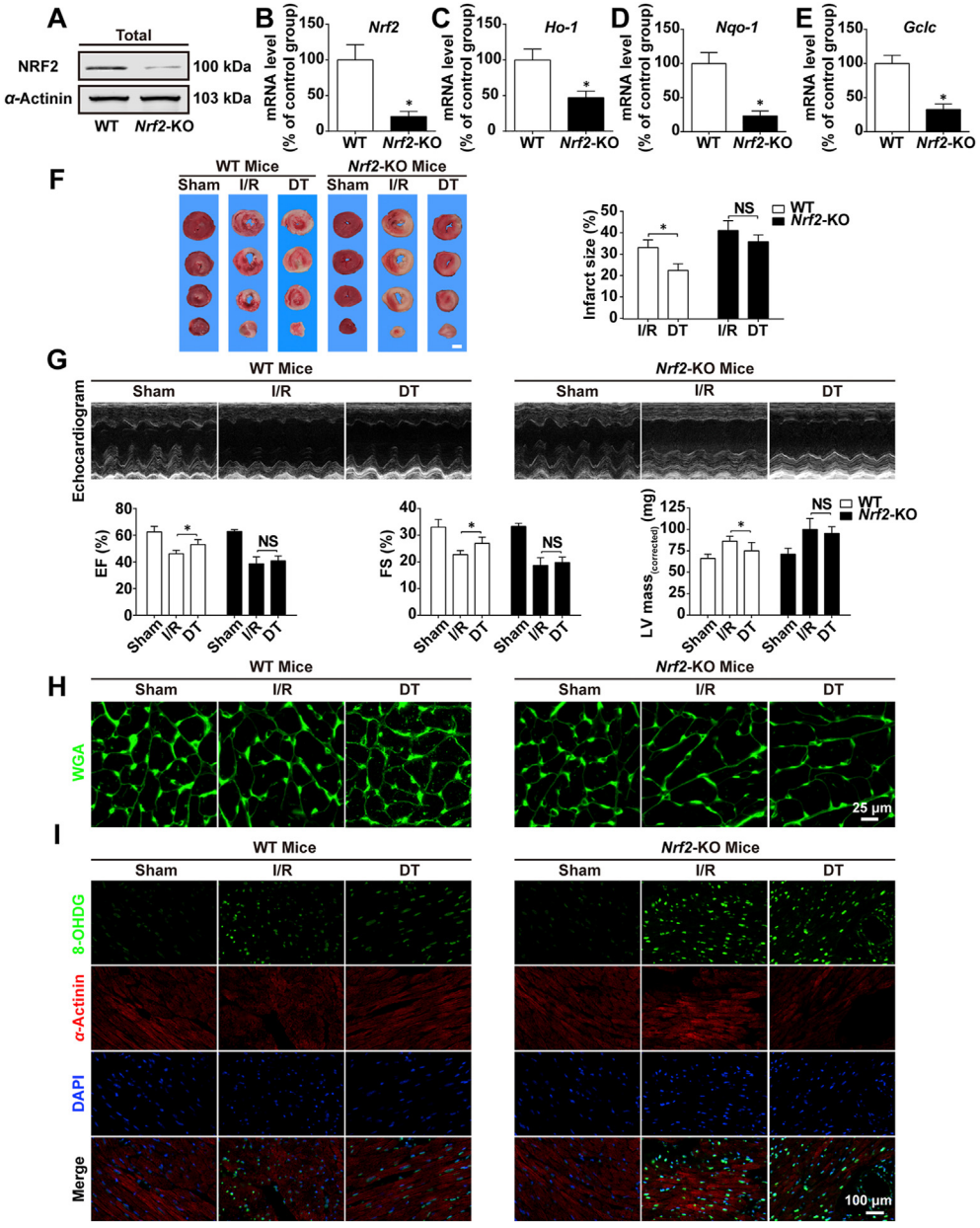

Figure 2 Genetically knockout of Nrf2 abolishes the cardioprotective effects of DT against MIRI. (A) and (B) Protein level and gene expression of *Nrf2* in cardiac tissues of wild type (WT) and *Nrf2*-KO mice ($n = 5$). (C)−(E) Gene expression of *Ho-1*, *Nqo-1* and *Gclc* in cardiac tissues of WT and *Nrf2*-KO mice ($n = 5$). (F) Representative images and calculated infarct size of the myocardium of WT and *Nrf2*-KO mice, scale bar = 2 mm ($n = 5$). (G) Echocardiogram of LV and the calculated results of EF, FS and LV mass ($n = 6$). (H) Representative images of WGA-stained LV sections, scale bar = 25 μm ($n = 5$). (I) Representative images of 8-OHDG/α-actinin/DAPI-stained LV sections, scale bar = 100 μm ($n = 5$). Data are expressed as mean ± SD, $^*P < 0.05$ *versus* WT group (B−E); $^*P < 0.05$ *versus* I/R group (F) and (G).

cardiomyocytes for the knockdown of *Nrf2* (Supporting Information Fig. S1A−S1D) and H/R stimulation was applied. Indicated by results from CELLROX staining, cell viability, LDH leakage and MDA assay, siRNA-based knockdown of *Nrf2* abolished DT-induced protective effects after H/R (vehicle-treated *vs.* DT-treated cells in *Nrf2* knockdown cells, cell viability: 45% *vs.* 52%, LDH leakage: 542% *vs.* 482% and MDA content: 7.0 μmol/g protein *vs.* 6.4 μmol/g protein (Fig. S1E−S1H). These results collectively validate that cardioprotection against MIRI offered by DT is dependent on activation of NRF2 signaling.

3.3. DT facilitates nuclear translocation and prevents degradation of NRF2 by phosphorylation at Ser40 via PKC-dependent mechanism

To dig into the regulatory mechanism of NRF2 activation, we firstly checked the induction of NRF2 nuclear retention in resting cells. DT in different concentrations was applied to HL-1 cardiomyocytes for 6 h, nuclear NRF2 levels were examined by Western blot and immunofluorescence. As a result, nuclear NRF2 level increased in response to DT pretreatment with a peak at

5 μmol/L (Fig. 3A and B). Consistently, transactivation of NRF2 downstream genes *Ho-1*, *Nqo-1* and *Gclc* were also significantly induced (Fig. 3C−E).

Next, since DT induced NRF2 translocation to the nucleus, we hypothesized that DT could affect the expression of nuclear import transporters. However, Western blot results show that DT did not significantly alter intracellular content of the well-defined NRF2 importing proteins, importin-α5 and importin-β1 (Supporting Information Fig. S2A and S2B). Additionally, immunofluorescent results indicate that cytoplasmic/nuclear distribution of importin-α5 and importin-β1 was also not evidently altered by DT (Fig. S2C and S2D), so there might exist other mechanisms. We show that apart from increased nuclear NRF2 level, total NRF2 content was also dose-dependently upregulated in response to DT treatment (Fig. 3F). Furthermore, DT increased total NRF2 content in the presence of protein synthesis inhibitor CHX (25 μmol/L), indicating that DT blocked the degradation of NRF2 (Fig. 3G), and DT decreased ubiquitin content in NRF2-immunoprecipitated sample (Fig. 3H). These results show that ubiquitination-dependent degradation of NRF2 was inhibited by DT, which was in accordance with a previous report. Since DT increased total NRF2 level and rendered nuclear accumulation, we hypothesized that there might be an upstream regulator convergently mediating these events. We firstly examined whether DT could promote NRF2 release by decreasing the expression of NRF2 inhibitor—KEAP1, but results show that protein level of KEAP1 was not significantly altered (Fig. 3I). We then turned to examine phosphorylation of NRF2 at Ser40, which is proposed to dissociate NRF2 from KEAP1 and enables its nuclear import. Surprisingly, NRF2 (Ser40) phosphorylation increased in response to DT stimulation (Fig. 3J). Among pleiotropic protein kinase families, PKC is putatively regarded to directly function on NRF2. As expected, specific PKC inhibitor Go-6983 largely blunted phosphorylation of NRF2 at Ser40 (Fig. 3K) and reversed DT-induced inhibition of NRF2 ubiquitination (Fig. 3L), collectively indicating that these modifications are dependent on PKC. In addition, Western blot experiments indicate that Go-6983 partially reversed NRF2 nuclear accumulation induced by DT, and NRF2 showed more retention outside the nucleus region (Fig. 3M). Finally, DT-induced upregulation of *Ho-1*, *Nqo-1* and *Gclc* mRNA level as well as beneficial effects were concordantly abrogated by Go-6983 (Supporting Information Fig. S3A−S3E).

In this section, we have identified, for the first time, PKC as a pivotal mediator that triggers DT-induced phosphorylation of NRF2 at Ser40, which mediates the release of NRF2 from KEAP1 and therefore facilitates nuclear import.

3.4. *PKC-δ-triggered NRF2 (Ser40) phosphorylation contributes to DT-induced NRF2 nuclear import*

Being shown that NRF2 nuclear import is dependent on PKC activation, we sought to clarify more specific modulatory mechanism of DT. The PKC family has several isoforms, among which PKC-α, PKC-δ, PKC-η and PKC-ε are most closely related to oxidative injury and cardioprotection. In order to confirm the exact isoform responsible for DT-induced NRF2 activation, siRNA targeting different *Pkc* isoforms was applied. Knockdown efficiency was firstly examined by Western blot experiment, and siRNA with high efficiency and specificity is chosen. Consequently, among all siRNA-treatment groups, only knockdown of *Pkc-δ* expression significantly reversed DT-induced NRF2 (Ser40) phosphorylation (Fig. 4A), indicating that PKC-δ might be the one that targets NRF2. PKC-δ is a PKC isoform closely involved in oxidative response, and its activity is regulated *via* multiple mechanisms including transcriptional regulation, membrane translocation and post-translational modifications. DT did not significantly increase intracellular protein content of PKC-δ (Fig. 4B), and immunofluorescent results indicate the absence of evident mitochondrial translocation of PKC-δ (Fig. 4C). Then we continued to examine its phosphorylation at Thr505, a conserved threonine residue that decided PKC-δ activity. As a result, PKC-δ retained a relatively low phosphorylation level at Thr505 in resting cardiomyocytes and could be upregulated by DT dose-dependently (Fig. 4D). Western blot experiments indicate that siRNA-dependent *Pkc-δ* knockdown decreased nuclear NRF2 level (Fig. 4F). Consistently, immunofluorescent experiments indicate that NRF2 nuclear accumulation induced by DT is also reversed, and NRF2 showed more retention outside the nucleus region (Fig. 4E), indicating its phosphorylation is dependent on PKC-δ activation. Finally, *Pkc-δ* knockdown abrogated DT-induced cardioprotection against H/R injury, manifested by exacerbated loss-of cell viability and LDH release (Fig. 4G and H).

Here we provide solid evidences demonstrating that PKC-δ activation is required for DT-induced NRF2 (Ser40) phosphorylation and subsequent nuclear import, phosphorylation of PKC-δ at Thr505 triggers NRF2-dependent antioxidant response that underlies the cytoprotective effects of DT.

3.5. *DT blocks Fyn-dependent NRF2 nuclear export via PKB/GSK-3β signaling*

Apart from nuclear import signals (NIS), intranuclear NRF2 level is also presided over by nuclear export signals (NES) that might compromise the antioxidant activity. For this reason, we speculated that combining DT with LMB, a nuclear export inhibitor, could yield a synergistic effect in nuclear accumulation of NRF2 and probably enhance therapeutic efficacy against oxidative stress. However, beyond our expectation, application of LMB (50 nmol/L) did not further increase nuclear NRF2 level in DT-treated cardiomyocytes (Fig. 5A). In the meanwhile, seeing that blocking nuclear import of NRF2 by inhibiting PKC-δ seemed incompetent to fully abolish DT-induced NRF2 nuclear accumulation, we thus hypothesized that besides PKC-δ-dependent nuclear import promotion, the nuclear export signaling of NRF2 might have also been occupied by DT. Supporting this hypothesis, DT delayed nuclear export of NRF2 in the presence of NIS inhibitor SN-50 (Fig. 5B), also directing us to investigate nuclear export-related mechanism.

Fyn, a tyrosine kinase, was reported to phosphorylate nuclear NRF2 at Tyr568 and promoted NRF2 export from nucleus, we evaluated whether Fyn could mediate DT-induced nuclear export of NRF2. Consistently, nuclear Fyn was downregulated by DT dose-dependently (Fig. 5C). Phosphorylation of Fyn was driven by its upstream kinase GSK-3β and positively regulates the nuclear translocation of Fyn. Western blot assays hinted that DT dose-dependently inactivated GSK-3β by phosphorylating at its Ser9 residue (Fig. 5D), which hindered nuclear accumulation of Fyn. As a potential regulator of GSK-3β activity, PKB was thereby investigated for its phosphorylation level at the canonical sites Ser473. As expected, DT significantly increased the protein phosphorylation of PKB at Ser473 (Fig. 5E). A specific PKB inhibitor MK-2206 (2 μmol/L) and a phosphorylation inhibitor for GSK-3β, DIF-3 (10 μmol/L) were employed to block the

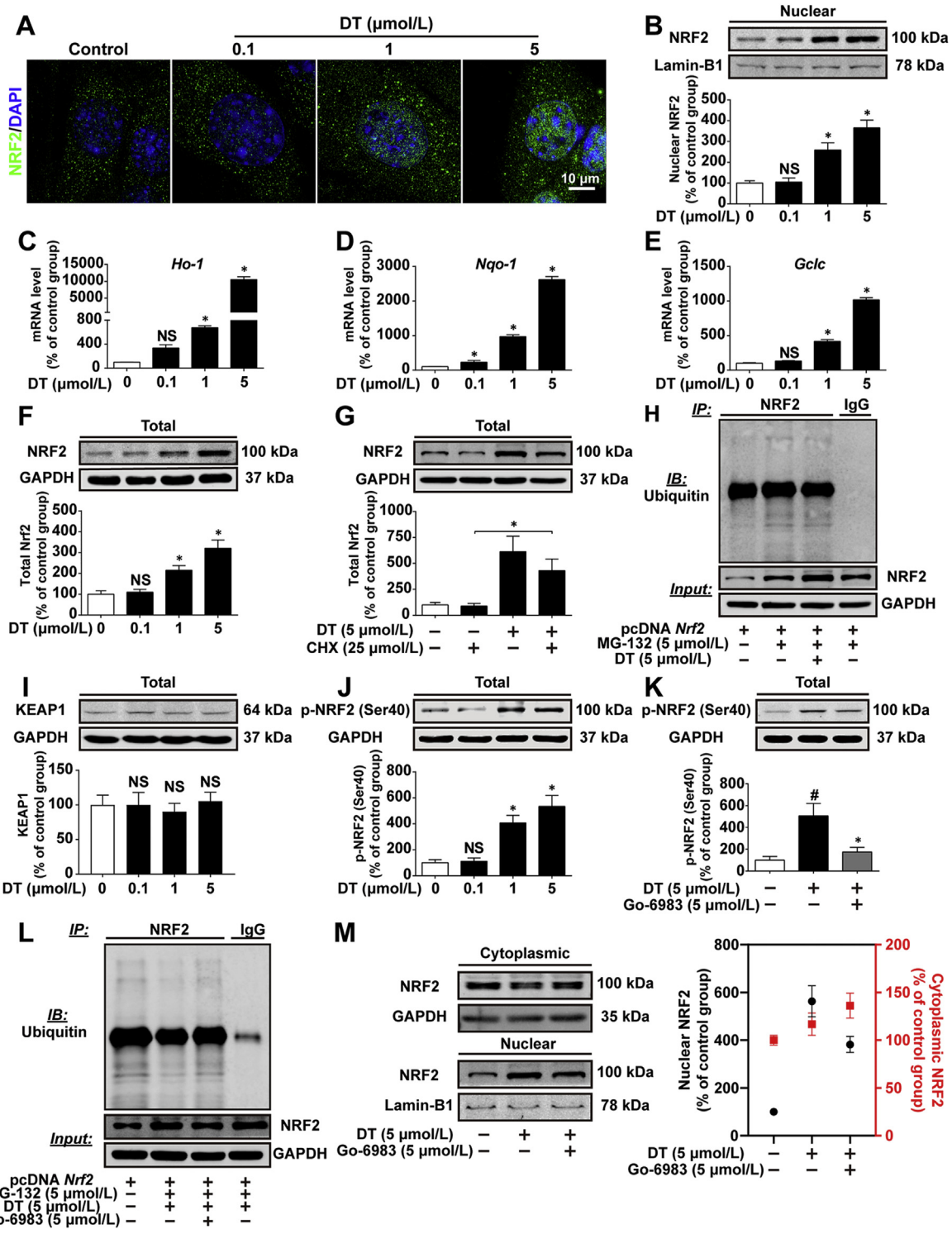

Figure 3 DT facilitates nuclear translocation and prevents degradation of NRF2 by phosphorylation at Ser40 *via* PKC-dependent mechanism. (A) Representative images of immunofluorescent staining of NRF2 in cardiomyocytes and the calculated intensity of nuclear NRF2, scale bar = 10 μm ($n = 5$). (B) Nuclear protein level of NRF2 in cardiomyocytes treated with DT in different concentrations ($n = 5$). (C)−(E) Gene expression of *Ho-1*, *Nqo-1* and *Gclc* determined by q-PCR experiment in cardiomyocytes ($n = 5$). (F) Total protein level of NRF2 ($n = 5$). (G) Total protein level of NRF2 in cardiomyocytes treated with vehicle or DT in the absence or presence of cycloheximide (CHX, 25 μmol/L; $n = 5$). (H) Ubiquitination analysis of NRF2 ($n = 3$). (I) Total protein level of KEAP1 ($n = 5$). (J) Protein phosphorylation of NRF2 at Ser40 ($n = 5$). (K) Protein phosphorylation of NRF2 at Ser40 in cardiomyocytes treated with DT in the absence and presence of Go-6983 ($n = 5$). (L) Ubiquitination analysis of NRF2 ($n = 3$). (M) Cytoplasmic and nuclear protein level of NRF2 in cardiomyocytes treated with DT in the absence and presence of Go-6983. Data are expressed as mean ± SD, $^*P < 0.05$ *versus* CHX group (B−F, J), $^*P < 0.05$ *versus* CHX group (G), $^{\#}P < 0.05$ *versus* control group, $^*P < 0.05$ *versus* DT group (K).

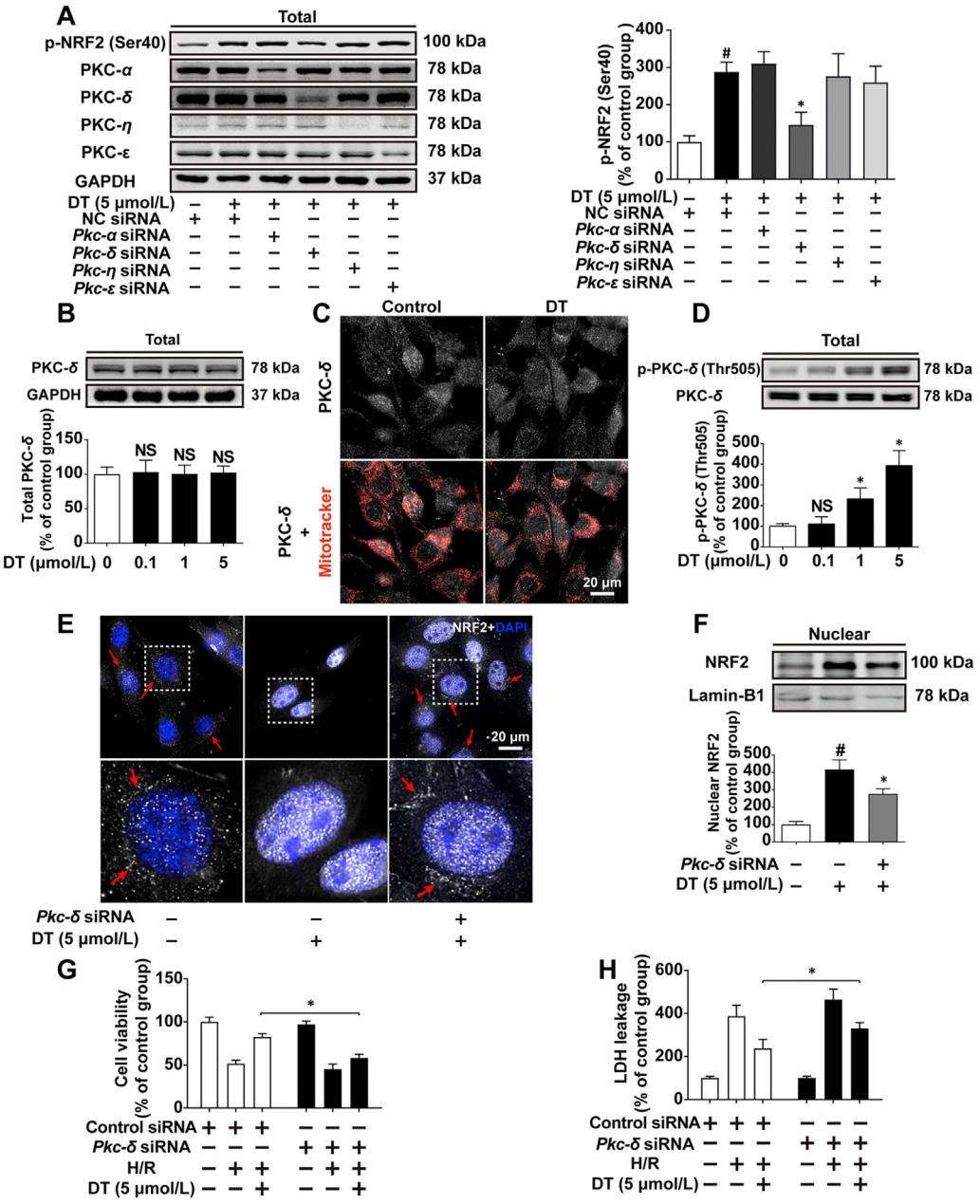

Figure 4 PKC-δ-triggered NRF2 (Ser40) phosphorylation contributes to DT-induced NRF2 release and nuclear import. (A) Protein phosphorylation of NRF2 at Ser40 upon respective knockdown of several primary PKC isoforms in cardiomyocytes ($n = 5$). (B) Total protein level of PKC-δ ($n = 5$). (C) Counterstaining of PKC-δ and intracellular mitochondria, scale bar = 20 μm ($n = 5$). (D) Protein phosphorylation of PKC-δ at Thr505 in cardiomyocytes treated with DT ($n = 5$). (E) Immunofluorescent staining of intracellular NRF2, scale bar = 20 μm ($n = 5$). (F) Nuclear protein level of NRF2 ($n = 5$). (G) and (H) Cell viability and extracellular LDH leakage of cardiomyocytes ($n = 5$). Data are expressed as mean ± SD, $^{\#}P < 0.05$ *versus* control group, $^{*}P < 0.05$ *versus* DT group (A) and (F); $^{*}P < 0.05$ *versus* control group (D); $^{*}P < 0.05$ *versus* indicated group (G) and (H).

phosphorylation of PKB and GSK-3β to examine the links between activation of PKB/GSK-3β/Fyn axis and nuclear NRF2 retention. Both application of MK-2206 or DIF-3 reversed DT-induced phosphorylation of GSK-3β at Ser9 and aggravated the nuclear accumulation of Fyn (Fig. 5G and H), resulting in augmented nuclear export signaling of NRF2, and consequently decreased nuclear NRF2 level (Fig. 5I). Phosphorylation of PKB was not evidently altered by DIF-3 treatment (Fig. 5F), which accords with previous findings that GSK-3β serves as a downstream substrate for PKB. These results demonstrate that apart from PKC-δ-dependent NRF2 nuclear import pathway, Fyn-dependent inhibition of NRF2 export signaling is blocked by DT through PKB/GSK-3β-related mechanism, which might synergize PKC-δ in augmenting the nuclear accumulation of NRF2. In order to capture above molecular changes induced by DT *in vivo*, we further investigated activation of PKC-δ and PKB/GSK-3β signaling in cardiac tissues from mice administered with DT. As a consequence, PKC-δ and PKB/GSK-3β were concordantly

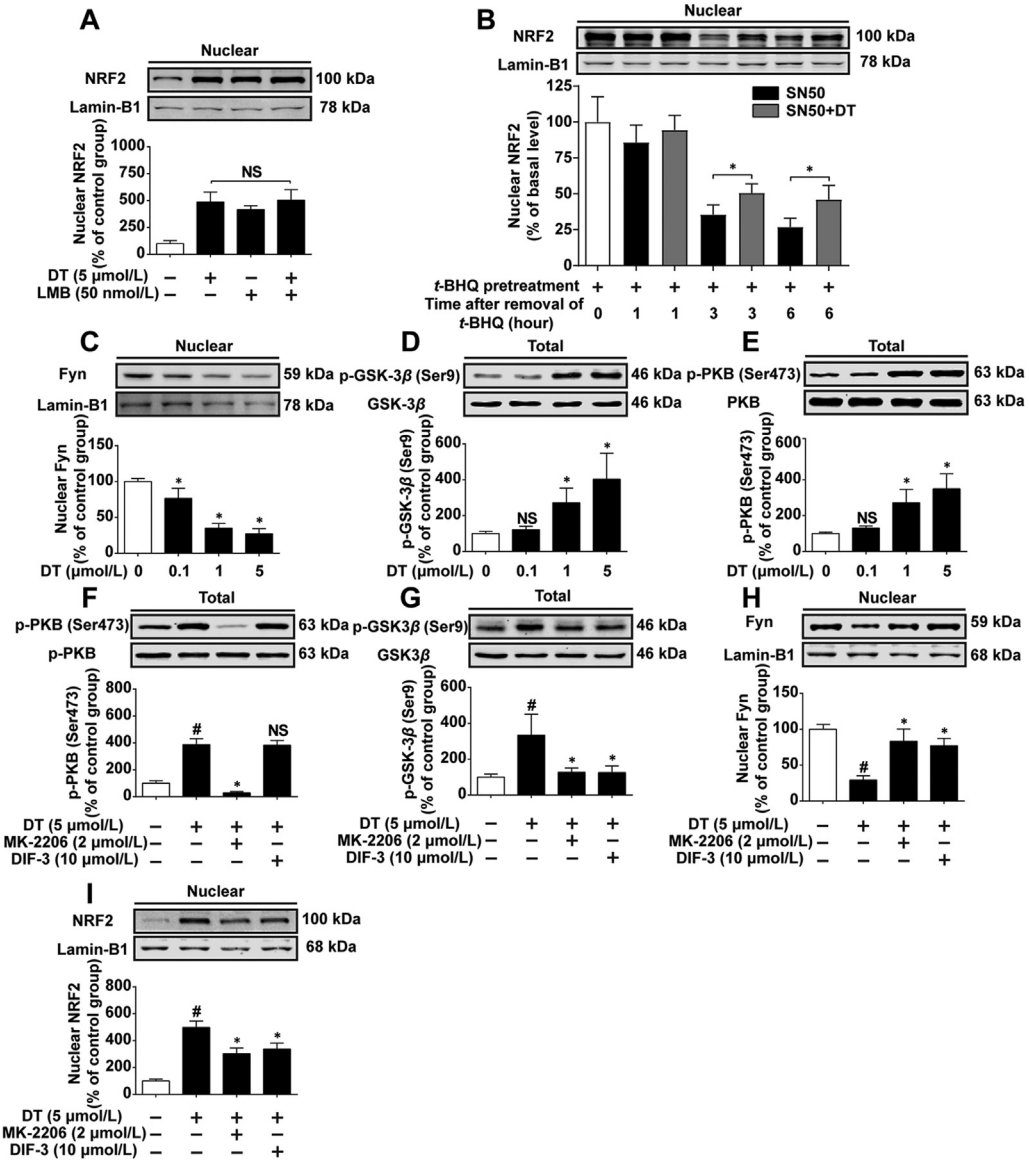

Figure 5 DT blocks Fyn-dependent NRF2 nuclear export *via* PKB/GSK-3β signaling. (A) Nuclear protein level of NRF2 in cardiomyocytes treated with DT or LMB, either alone or in combination ($n = 5$). (B) Nuclear protein level of NRF2 in cardiomyocytes treated with SN50, either alone or in combination with DT ($n = 5$). (C)−(E) Nuclear protein level of Fyn, protein phosphorylation of GSK-3β (Ser9) and PKB (Ser473) in cardiomyocytes treated with DT ($n = 5$). (F) and (G) Protein phosphorylation of PKB (Ser473) and GSK-3β (Ser9) in cardiomyocytes treated with DT or MK-2206 or DIF-3, either alone or in combination ($n = 5$). (H) and (I) Nuclear protein level of Fyn and NRF2 in cardiomyocytes treated with DT or MK-2206 or DIF-3, either alone or in combination ($n = 5$). Data are expressed as mean ± SD, $^*P < 0.05$ *versus* indicated group (B); $^*P < 0.05$ *versus* control group (C)−(E); $^{\#}P < 0.05$ *versus* DT group, $^*P < 0.05$ *versus* DT group (F)−(I).

activated in a dose-dependent manner (Supporting Information Fig. S4A−S4C), further supporting our findings in cellular experiments.

3.6. PKB/GSK-3β synergizes PKC-δ signaling in convergently promoting DT-induced NRF2 nuclear retention and conferring potentiated protection against oxidative injury

Being implicated that both PKC-δ and PKB/GSK-3β/Fyn signaling were occupied in DT-treated cells, we tried to clarify the functional links. Despite that Go-6983 abrogated activation of PKC-δ (Fig. 6B), no significant changes were observed in neither phosphorylation of PKB or GSK-3β nor nuclear Fyn content (Fig. 6A and E). Meanwhile, DT-induced phosphorylation of PKC-δ was not evidently altered by PKB inhibitor MK-2206 (Fig. 6B), these results collectively indicate that the phosphorylation of PKC-δ and PKB/GSK-3β/Fyn might operate independently. We further examined whether PKB activation altered NRF2 nuclear import by directly phosphorylating NRF2 at Ser40. In resting cardiomyocytes, no significant spatial co-localization was found between p-PKB and NRF2. Although DT upregulated intracellular NRF2 and p-PKB

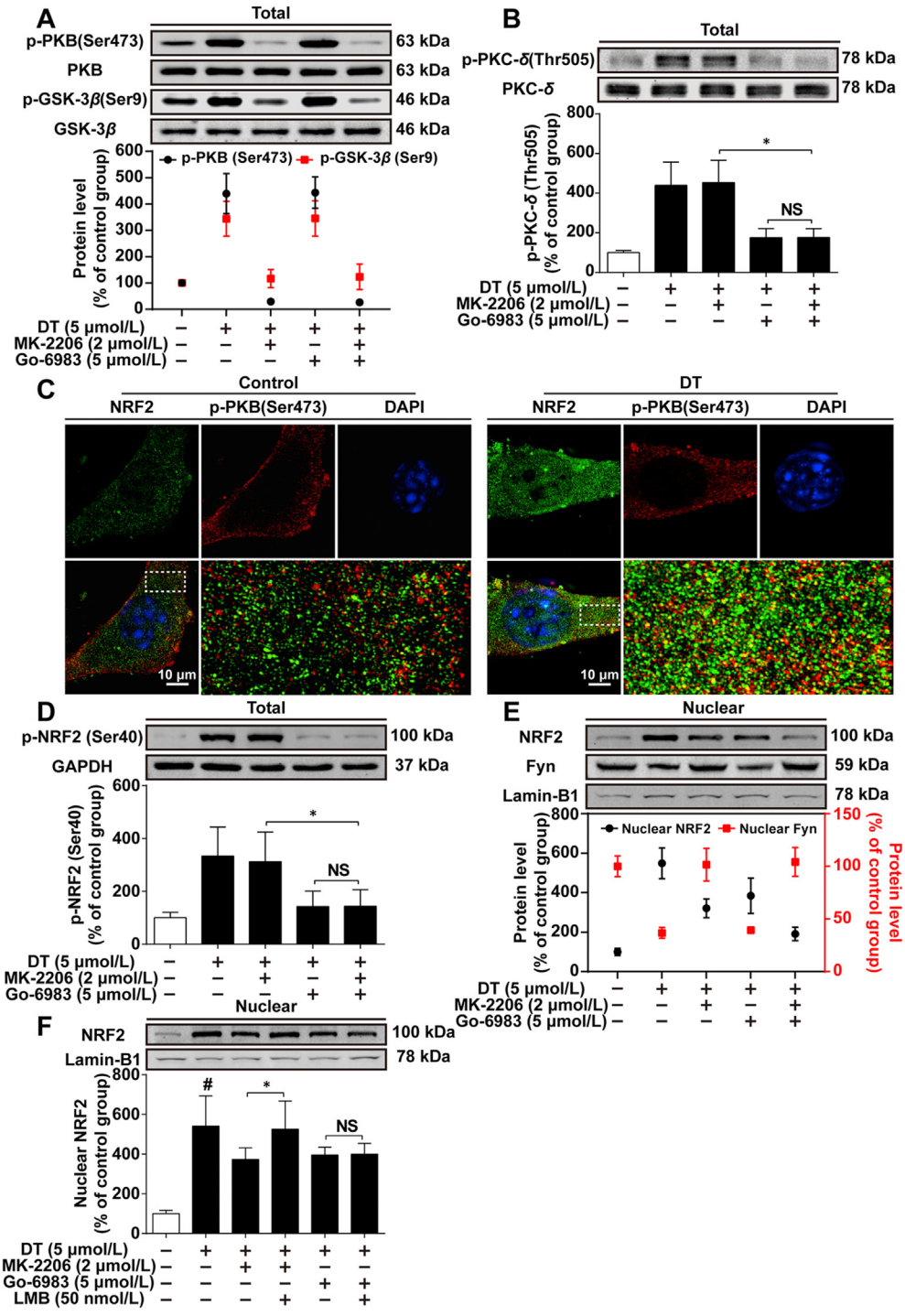

Figure 6 PKB/GSK-3β synergizes PKC-δ signaling in convergently promoting DT-induced NRF2 nuclear retention and conferring potentiated protection against oxidative injury. (A) and (B) Total protein level of phosphorylated PKB (Ser473), phosphorylated GSK-3β (Ser9) and phosphorylated PKC-δ (Thr505) in cardiomyocytes treated with DT or MK-2206 or Go-6983, either alone or in combination ($n = 5$). (C) Co-localization analysis of phosphorylated PKB (Ser473) and NRF2 using ultra-resolution microscopy. (D) and (E) Total protein level of phosphorylated NRF2 (Ser40) and nuclear protein level of NRF2 and Fyn in cardiomyocytes treated with DT or MK-2206 or Go-6983, either alone or in combination ($n = 5$). (F) Nuclear protein level of NRF2 in cardiomyocytes treated with DT, MK-2206, Go-6983 or LMB, either alone or in combination ($n = 5$). Data are expressed as mean ± SD, $^*P < 0.05$ *versus* indicated treatment.

(Ser473) level, it failed to induce evident co-localization of both protein (Fig. 6C). Phosphorylation of NRF2 (Ser40) was not reversed by MK-2206 (Fig. 6D), further demonstrating that NRF2 (Ser40) phosphorylation is independent of PKB activation.

We further determined the contribution of PKC-δ/NRF2 (Ser40) and PKB/GSK-3β/Fyn axis in inducing NRF2 nuclear retention. Combination of Go-6983 and MK-2206 exhibited a more potent suppressing effect on nuclear NRF2 content (Fig. 6E) and NRF2-downstream ARE genes (Supporting Information Fig. S5A−S5C).

Combining both inhibitors additively attenuated antioxidative-associated protective effects, evidenced by the highest LDH leakage and MDA content as well as the lowest cell viability among all medication groups (Fig. S5D−S5F). Finally, we tested whether restrained nuclear NRF2 retention by Go-6983 or MK-2206 could be rescued by LMB. A significant increase of nuclear NRF2 level is induced by LMB in MK-2206 and DT-treated cardiomyocytes other than Go-6983 and DT-treated cells (Fig. 6F). Hence, it could be conceivably concluded that DT-induced activation of PKB signaling basically contributed to the inhibition of NRF2 export signaling while PKC-δ merely regulated it.

These data manifest independent mode of actions of PKC-δ/NRF2 (Ser40) and PKB/GSK-3β signaling in regulating cytoplasmic/nuclear NRF2 translocation. Both pathways synergistically augment nuclear NRF2 accumulation, which might be a major contributor to DT-provided therapeutic effects.

3.7. *Co-activation of PKC and PKB signaling effectively attenuates I/R injury in a NRF2-dependent manner*

Blocking PKB/GSK-3β and PKC-δ largely abolished the NRF2 induction activity as well as cardioprotection of DT, we wondered whether co-activation of PKC-δ and PKB signaling could phenocopy the beneficial effects of DT in a NRF2-dependent manner. Specific PKC activator phorbol 12-myristate 13-acetate (PMA) was therefore applied to cardiomyocytes in combination with PKB activator SC79, and we tested whether this combination could protect cardiomyocytes from H/R injury. Consequently, PMA plus SC79 dose-dependently rescued cardiomyocytes from H/R injury (Fig. 7A and B) while *Nrf2* knockdown nullified the protective effects of this combination (Fig. 7C and D), demonstrating NRF2 dependency. Furthermore, whether this rationale is applicable *in vivo* also attracts our interests. To specifically knockdown *Nrf2* in cardiac tissue, AAV9-based shRNA delivery was applied[34], and a *c-Tnt* promoter was inserted to increase cardiac specificity (Supporting Information Fig. S6A). Cardiac-specific *Nrf2* knockdown was validated 3 weeks after AAV9 injection by both PCR and Western blot methods (Fig. S6B and S6C) and mice were subjected to subsequent I/R experiments. As a consequence, PMA (0.2 mg/kg) plus SC79 (2 mg/kg) significantly ameliorates MIRI in AAV9-control shRNA-treated mice, indicated by evident decrease in myocardial infarct size, preserved cardiac functions and improved oxidative injury. However, therapeutic efficacy of this combination was compromised in AAV9-*Nrf2* shRNA-treated animals, indicating that NRF2 is required, at least in part, for protection provided by PMA plus SC79. These results collectively support that the rationale of PKC and PKB signaling coactivation can effectively protect cardiomyocytes against ischemia/reperfusion injury in a NRF2-dependent manner.

4. Discussion

Therapeutic benefits of percutaneous coronary intervention have long been hindered by myocardial reperfusion injury[35]. Since ROS outburst is a pivotal initiator for MIRI, it is essential to improve post-ischemic prognosis by modulating redox homeostasis[36]. Ample evidence indicates that genetical and pharmacological activations of NRF2 uniformly protect against ischemic heart injuries in animal models while loss of NRF2 exacerbates heart failure following myocardial infarction[37,38], collectively highlighting the importance of NRF2 in attenuating ischemic heart diseases, and application of effective NRF2-inducer might provide benefits for the treatment of MIRI. A synthetic NRF2 inducer bardoxolone has previously entered phase III clinical trial, but was latterly withdrawn for potential cardiovascular side effects[39]. Therefore, applying naturally-derived NRF2 inducers from clinically-effective herbal medicines might be an alternative approach. DT is an active constituent in *S. miltiorrhiza,* which has been widely applied in ancient and modern clinical settings[40,41]. A previous study has reported cardioprotection of DT *via* inhibition of arachidonic acid ω-hydroxylase, while the validation of direct links is lacking. In other eukaryotes like skin cells and pneumonocytes, DT also provides potential beneficial effects associated with NRF2 regulation, and the mechanism is explained by inhibiting ubiquitination-dependent degradation. However, the mechanism for inhibiting NRF2 degradation and whether NRF2 directly mediated the therapeutic effects of DT still remains unrevealed.

In line with previously established links between oxidative stress and MIRI[42], our study shows that I/R initiates severe oxidative injury. Importantly, although NRF2 activation is adaptively upregulated after I/R (about 2-fold, Fig. 1F), I/R still causes 34% ultimate infarct size (Fig. 1B) that triggers subsequent cardiac dysfunction and hypertrophic response (Fig. 1C). Importantly, DT induces NRF2 nuclear accumulation to a more potent level (about 6-fold) in the myocardium and significantly relieves oxidative injury (indicated by decreased 8-OHDG intensity), contributing to much improved myocardial infarct size (about 23%) and ventricular functions (Fig. 1B−F). Consistently, our *in vitro* study shows that increased intracellular ROS generation after H/R insult impairs cell viability along with cytomembrane integrity in cardiomyocytes, and these detrimental effects were markedly attenuated by pretreatment of DT (Fig. 1G−J). Since DT pretreatment shows ameliorated oxidative injury associated with NRF2 upregulation, we further examined the functional links *in vivo* and *in vitro*. Genetically knockout of *Nrf2* downregulates gene expression of *Ho-1*, *Nqo-1* and *Gclc* (Fig. 2C−E), slightly exaggerating oxidative injury and cardiac functions in I/R-operated mice (Fig. 2F−I), which accord with results from a previous study[43]. DT fails to improve the final infarct size and subsequent cardiac remodeling in *Nrf2*-KO mice after I/R operations, demonstrating that the functional integrity of NRF2 is required for cardioprotection of DT. Accordantly, DT-induced beneficial effects are also abolished in *Nrf2*-siRNA-treated cardiomyocytes (Fig. S1E−S1H), further supporting the pivotal role of NRF2 in therapeutic efficacy of DT. Above results demonstrate that DT-induced further upregulated NRF2 signaling is able to combat I/R injury, and we confirm the functional links between NRF2 induction and cardioprotection of DT pretreatment for the first time.

A fundamental finding of this work is comprehensive survey of distinct mechanisms by which DT might activate NRF2 signaling. Both expression and intracellular localization of importin-α5 and importin-β1 show little alteration (Fig. S2A−S2D), indicating insignificant involvement of importins. In consistent with previous findings, we also notice that DT prevents NRF2 from degradation, then another question arises that through which upstream molecule this process is triggered. Results from our preliminary results indicate that DT does not affect basal expression of KEAP1, so other possibility should be considered. Ser40 of NRF2 is located in the N-terminal Neh2 domain that interacts with KEAP1, and a previous report indicates its phosphorylation can release NRF2

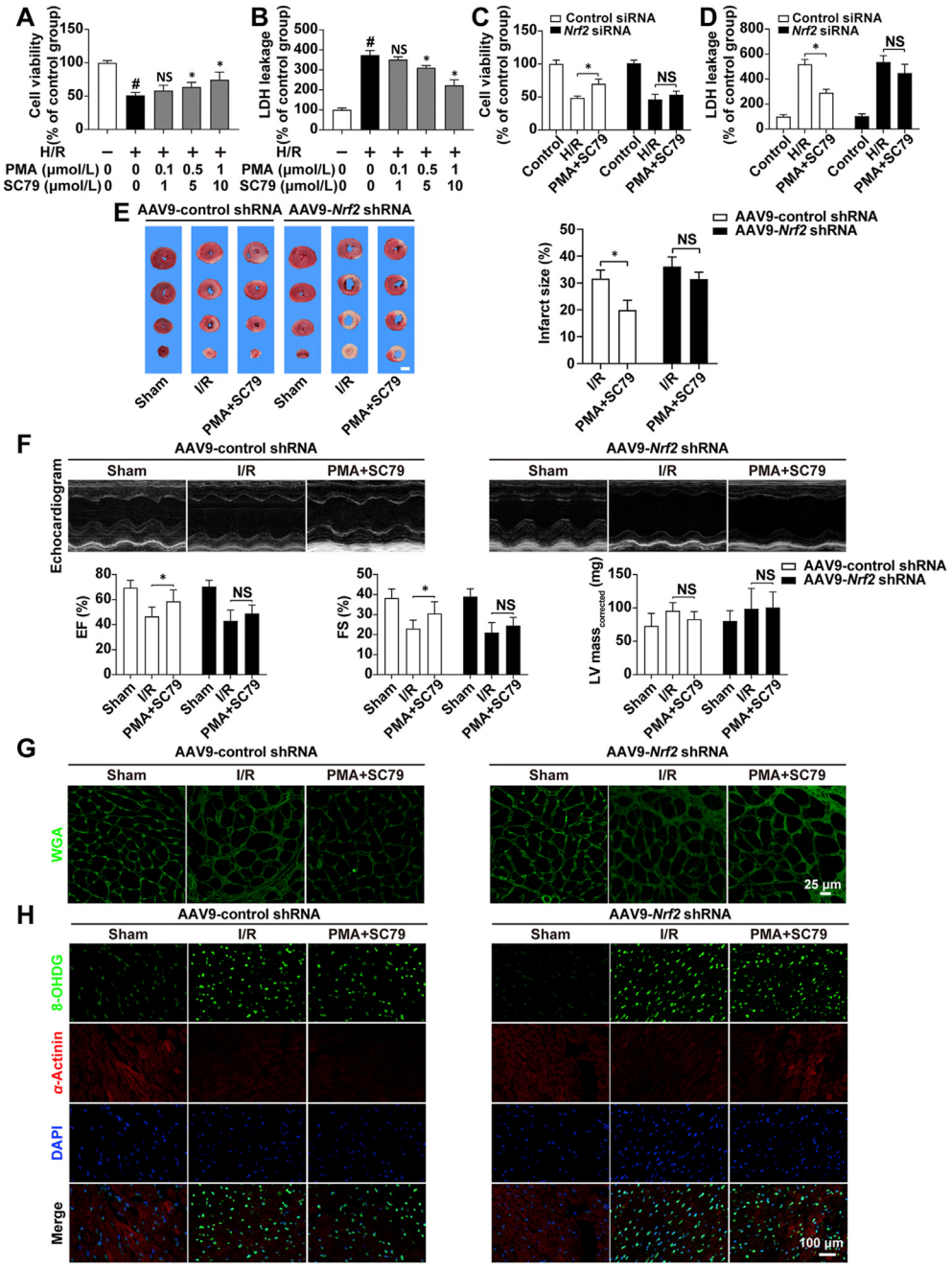

Figure 7 Co-activation of PKC and PKB signaling effectively attenuates I/R injury in a NRF2-dependent manner. (A) and (B) Cell viability and extracellular LDH leakage in cardiomyocytes treated with combination of PMA+SC79 ($n = 5$). (C) and (D) Cell viability and extracellular LDH leakage in control and *Nrf2*-knockdown cardiomyocytes treated with PMA (1 μmol/L) plus SC79 (10 μmol/L) ($n = 5$). (E) Representative images and calculated infarct size of the myocardium of control shRNA and *Nrf2* shRNA-treated mice treated with vehicle or PMA (0.2 mg/kg) plus SC79 (2 mg/kg), scale bar = 2 mm ($n = 5$ animals each group). (F) Echocardiogram of LV and the calculated results of EF, FS and LV mass ($n = 5$ animals each group). (G) Representative images of WGA-stained LV sections, scale bar = 25 μm ($n = 5$ animals each group). (H) Representative images of 8-OHDG/α-actinin/DAPI-stained LV sections, scale bar = 100 μm ($n = 5$ animals each group). Data are expressed as mean ± SD, $^{\#}P < 0.05$ *versus* control group; $^{*}P < 0.05$ *versus* H/R or I/R group.

from KEAP1 and renders nuclear import. DT induced NRF2 Ser40 phosphorylation accompanied by intracellular accumulation *via* degradation inhibition (Fig. 3F, G and J). A putative link has been assumed to exist between NRF2 Ser40 phosphorylation and PKC, and PKC inhibitor Go-6983 abolishes NRF2 Ser40 phosphorylation and exacerbates ubiquitination (Fig. 3K and L). DT-induced transactivation of NRF2 downstream genes and beneficial effects are concordantly nullified (Fig. S3A−S3E), collectively demonstrating DT promotes NRF2 nuclear import and exert cardioprotective effects dependent on PKC.

Another important finding of this study is we identified PKC-δ from several ubiquitously expressed and functionally important PKC isoforms in cardiomyocytes as the mediator responsible for NRF2 nuclear import. Interestingly, although PKC-ε is commonly implicated in beneficial effects against reperfusion injury[44,45], it seems indirectly involved in NRF2 nuclear import. Only knockdown of *Pkc-δ*, which is closely related to cellular responses to oxidative stress[46], evidently abolished DT-induced NRF2 Ser40 phosphorylation (Fig. 4A). PKC-δ activity is regulated under diverse mechanisms including membrane translocation as well as post-translational modifications[47,48]. Unexpectedly, DT does not evidently affect expression along with mitochondrial translocation of PKC-δ (Fig. 4A), while the phosphorylation at Thr505 within its activation loop is dose-dependently induced. PKC-δ (Thr505) phosphorylation is "barely there" in resting cardiomyocytes and elevates in response to DT stimulation (Fig. 4B). Immunofluorescent analysis of the intracellular localization of NRF2 demonstrates that NRF2 shows more retention in cytoplasm upon nullification of PKC-δ (Fig. 4D−F), and preservation of cell viability and membrane integrity are concordantly reversed. These results provide strong evidence that DT-induced beneficial effects through NRF2 activation are dependent on PKC-δ activity (Fig. 3H−L).

Application of nuclear export inhibitor LMB does not synergize DT in promoting NRF2 nuclear accumulation (Fig. 5A) and nuclear import inhibitor SN50 failed to completely block DT-induced NRF2 nuclear accumulation, suggesting that nuclear export process of NRF2 might be inhibited by DT (Fig. 5B). Phosphorylation of nuclear NRF2 at Tyr568 promotes its export, which is dependent on intranuclear Fyn, a member of SRC tyrosine kinase family[49,50]. And GSK-3β is implicated as the kinase of Fyn by phosphorylating and promoting its nuclear accumulation. We demonstrate that DT inactivates GSK-3β by phosphorylating at Ser9 and thus hinders Fyn accumulation (Fig. 5C and D). As a result, less intranuclear Fyn allows NRF2 unimpeded binding to ARE. GSK-3β is a direct substrate with its activity regulated by active form of PKB, and Ser473 is an active site of PKB that targets cellular survival procedures[51,52]. DT significantly phosphorylates PKB at Ser473 (Fig. 5E), consistent with a previous conclusion that phosphorylation of PKB at Ser473 is sufficient to inactivate GSK-3β[53]. Indeed, MK-2206 reverses GSK-3β Ser9 phosphorylation. Unexpectedly, although MK-2206 blocks PKB (Ser473) phosphorylation to much lower level compared to resting cells, GSK-3β phosphorylation is not downregulated to comparable extent, indicating that basal GSK-3β activity might be independent of PKB (Fig. 5F and G). Additionally, DIF-3[54], a specific inhibitor for GSK-3β, does not affect PKB Ser473 phosphorylation but still promotes Fyn nuclear accumulation (Fig. 5F−H), convincing that PKB Ser473 phosphorylation acts upstream of GSK-3β/Fyn pathway in inhibiting NRF2 nuclear exclusion.

In addition, we have examined the possible interaction between PKB and PKC in modulating NRF2 nuclear retention in DT-stimulated cardiomyocytes. Although both kinases are ubiquitously expressed in cytoplasm and might be crosslinked[55,56], while whether the interplay between them is reciprocal in regulating NRF2 activity has not been examined. In the presence of DT, Go-6983 does not affect the phosphorylation cascade of PKB/GSK-3β axis and only partially reverses NRF2 antioxidative response, and meanwhile MK-2206 changes little in PKC-δ (Thr505, Fig. 6A and B), suggesting absence of direct "kinase−substrate" relationship between PKC-δ and PKB. More importantly, activated PKB does not co-localize NRF2 and MK-2206 failed to significantly reverse NRF2 (Ser40) phosphorylation (Fig. 6C and D), further decreasing the possibility that PKB directly phosphorylates NRF2 Ser40. Combination of Go-6983 and MK-2206 additively blunts increase of nuclear NRF2 content and ARE gene expression (Fig. 6E and Fig. S5A−S5C), and as a consequence, largely abolishes beneficial effects of DT (Fig. S5D−S5F), strongly implicating the unique contributions of both PKC-δ and PKB/GSK-3β/Fyn signaling to nuclear NRF2 accumulation. Additionally, LMB rescues reversion of nuclear NRF2 accumulation in MK-2206+DT treated cardiomyocytes but elicits no response in Go-6983+DT-treated cells, again implying unique roles of PKC-δ and PKB/GSK-3β/Fyn axis in mediating NRF2 nuclear import/export regulation (Fig. 6F). Compared with previous findings that PKB signaling might augment the biological activities of NRF2[57,58], our results also implicate that NRF2 activity is enhanced in the presence of activated PKB signaling. Together with identifying the functions of PKC-δ, our results highlight the ability of DT to exploit both nuclear import and export procedure of NRF2 in the treatment of reperfusion injury harboring redox homeostasis alterations. Finally, combinatorial application of PKC activator PMA and PKB activator SC79 exerted solid cardioprotection both *in vitro* and *in vivo*, while *Nrf2* knockdown attenuated the beneficial effects of this combination. These results provide additional implications that modulating NRF2 signaling by coactivation of PKC and PKB signaling might be a feasible therapeutic strategy to protect heart from ischemia/reperfusion injury.

5. Conclusions

The present study provides strong evidences *in vivo* and *in vitro* that therapeutic benefits of DT against MIRI largely depend on activation of NRF2 signaling. Importantly, activation of PKC-δ is demonstrated as a key mechanism through which DT promotes NRF2 nuclear import. We also unveil the role of PKB/GSK-3β/Fyn signaling in augmenting NRF2 activity by delaying its nuclear export. The independent regulation of PKC-δ and PKB/GSK-3β/Fyn signaling by DT provides a convergent mechanism for NRF2 nuclear accumulation, which dominates the protective effects of DT against MIRI *via* maintaining redox homeostasis. By determining the NRF2-dependent cardioprotective effects of PMA plus SC79, this study also introduces a promising therapeutic strategy for I/R injury by coactivation of PKC and PKB and demonstrate this strategy to enhance NRF2 activity in cardiomyocytes.

Acknowledgments

This work was supported by the National Key R&D Program of China (No. 2019YFC1711000), National Natural Science Foundation of China (81421005 and 81722048), 111 Project (B16046, China), "Double First-Class" University Project (CPU2018GF04, China) and the Qing Lan Project of Jiangsu Province (China).

Author contributions

Hao Zeng and Lingling Wang planned and performed experiments, analyzed data and drafted the manuscript. Ting Pan, Yinghua Yu and Jingxia Lu helped perform *in vivo* experiments. Hao Zeng performed genotyping and inhibitor experiments. Ping Zhou provided reagent,

helped design experiments. Jiawei Zhang helped edit manuscript. Ping Li and Hua Yang, the principal investigators, conceived the scientific ideas, oversaw the project, designed the experiments and refined the manuscript.

Conflicts of interest

The authors declare no conflicts of interest in this work.

Appendix A. Supporting information

Supporting data to this article can be found online at https://doi.org/10.1016/j.apsb.2020.09.006.

References

1. Levine GN, Bates ER, Blankenship JC, Bailey SR, Bittl JA, Cercek B, et al. 2015 ACC/AHA/SCAI focused update on primary percutaneous coronary intervention for patients with ST-elevation myocardial infarction: An update of the 2011 ACCF/AHA/SCAI Guideline for Percutaneous Coronary Intervention and the 2013 ACCF/AHA Guideline for the Management of ST-Elevation Myocardial Infarction. *J Am Coll Cardiol* 2016;**67**:1235–50.
2. Eltzschig HK, Eckle T. Ischemia and reperfusion—from mechanism to translation. *Nat Med* 2011;**17**:1391–401.
3. Yellon DM, Hausenloy DJ. Myocardial reperfusion injury. *N Engl J Med* 2007;**357**:1121–35.
4. Murphy E, Steenbergen C. Mechanisms underlying acute protection from cardiac ischemia–reperfusion injury. *Physiol Rev* 2008;**88**:581–609.
5. Espinosa-Diez C, Miguel V, Mennerich D, Kietzmann T, Sanchez-Perez P, Cadenas S, et al. Antioxidant responses and cellular adjustments to oxidative stress. *Redox Biol* 2015;**6**:183–97.
6. Motohashi H, Yamamoto M. Nrf2–Keap1 defines a physiologically important stress response mechanism. *Trends Mol Med* 2004;**10**:549–57.
7. Rushworth SA, Ogborne RM, Charalambos CA, O'Connell MA. Role of protein kinase C delta in curcumin-induced antioxidant response element-mediated gene expression in human monocytes. *Biochem Bioph Res Co* 2006;**341**:1007–16.
8. Christie M, Chang CW, Rona G, Smith KM, Stewart AG, Takeda AA, et al. Structural biology and regulation of protein import into the nucleus. *J Mol Biol* 2016;**428**:2060–90.
9. Theodore M, Kawai Y, Yang JQ, Kleshchenko Y, Reddy SP, Villalta F, et al. Multiple nuclear localization signals function in the nuclear import of the transcription factor NRF2. *J Biol Chem* 2008;**283**:8984–94.
10. Bloom DA, Jaiswal AK. Phosphorylation of Nrf2 at Ser40 by protein kinase C in response to antioxidants leads to the release of Nrf2 from INrf2, but is not required for Nrf2 stabilization/accumulation in the nucleus and transcriptional activation of antioxidant response element-mediated NAD(P)H:quinone oxidoreductase-1 gene expression. *J Biol Chem* 2003;**278**:44675–82.
11. Lo SC, Hannink M. PGAM5 tethers a ternary complex containing Keap1 and Nrf2 to mitochondria. *Exp Cell Res* 2008;**314**:1789–803.
12. O'Mealey GB, Plafker KS, Berry WL, Janknecht R, Chan JY, Plafker SM. A PGAM5–KEAP1–Nrf2 complex is required for stress-induced mitochondrial retrograde trafficking. *J Cell Sci* 2017;**130**:3467–80.
13. Jain AK, Jaiswal AK. GSK-3β acts upstream of Fyn kinase in regulation of nuclear export and degradation of NF-E2 related factor 2. *J Biol Chem* 2007;**282**:16502–10.
14. Han JY, Fan JY, Horie Y, Miura S, Cui DH, Ishii H, et al. Ameliorating effects of compounds derived from *Salvia miltiorrhiza* root extract on microcirculatory disturbance and target organ injury by ischemia and reperfusion. *Pharmacol Therapeut* 2008;**117**:280–95.
15. Xia Z, Gu J, Ansley DM, Xia F, Yu J. Antioxidant therapy with *Salvia miltiorrhiza* decreases plasma endothelin-1 and thromboxane B2 after cardiopulmonary bypass in patients with congenital heart disease. *J Thorac Cardiovasc Surg* 2003;**126**:1404–10.
16. Cheng TO. Cardiovascular effects of Danshen. *Int J Cardiol* 2007;**121**:9–22.
17. Meng ZJ, Wang C, Meng LT, Bao BH, Wu JH, Hu YQ. Sodium tanshinone IIA sulfonate attenuates cardiac dysfunction and improves survival of rats with cecal ligation and puncture-induced sepsis. *Chin J Nat Med* 2018;**16**:846–55.
18. Jiang B, Li D, Deng Y, Teng F, Chen J, Xue S, et al. Salvianolic acid A, a novel matrix metalloproteinase-9 inhibitor, prevents cardiac remodeling in spontaneously hypertensive rats. *PLoS One* 2013;**8**.e59621.
19. Wu WY, Wang WY, Ma YL, Yan H, Wang XB, Qin YL, et al. Sodium tanshinone IIA silate inhibits oxygen-glucose deprivation/recovery-induced cardiomyocyte apoptosis *via* suppression of the NF-κB/TNF-α pathway. *Br J Pharmacol* 2013;**169**:1058–71.
20. Song J, Zhang W, Wang J, Yang H, Zhou Q, Wang H, et al. Inhibition of FOXO3a/BIM signaling pathway contributes to the protective effect of salvianolic acid A against cerebral ischemia/reperfusion injury. *Acta Pharm Sin B* 2019;**9**:505–15.
21. Jiang L, Zeng H, Ni L, Qi L, Xu Y, Xia L, et al. HIF-1α preconditioning potentiates antioxidant activity in ischemic injury: The role of sequential administration of dihydrotanshinone I and protocatechuic aldehyde in cardioprotection. *Antioxid Redox Signal* 2019;**31**:227–42.
22. Tao S, Justiniano R, Zhang DD, Wondrak GT. The Nrf2-inducers tanshinone I and dihydrotanshinone protect human skin cells and reconstructed human skin against solar simulated UV. *Redox Biol* 2013;**1**:532–41.
23. Wei Y, Xu M, Ren Y, Lu G, Xu Y, Song Y, et al. The cardioprotection of dihydrotanshinone I against myocardial ischemia–reperfusion injury *via* inhibition of arachidonic acid omega-hydroxylase. *Can J Physiol Pharmacol* 2016;**94**:1267–75.
24. Gonzalez MC, Marteau C, Franchi J, Migliore-Samour D. Cytochrome P450 4A11 expression in human keratinocytes: Effects of ultraviolet irradiation. *Br J Dermatol* 2001;**145**:749–57.
25. Zhang JM, Wang XH, Hao LH, Wang H, Zhang XY, Muhammad I, et al. Nrf2 is crucial for the down-regulation of Cyp7a1 induced by arachidonic acid in Hepg2 cells. *Environ Toxicol Pharmacol* 2017;**52**:21–6.
26. Wu JH, Hodgson JM, Clarke MW, Indrawan AP, Barden AE, Puddey IB, et al. Inhibition of 20-hydroxyeicosatetraenoic acid synthesis using specific plant lignans: *In vitro* and human studies. *Hypertension* 2009;**54**:1151–8.
27. Tao S, Zheng Y, Lau A, Jaramillo MC, Chau BT, Lantz RC, et al. Tanshinone I activates the Nrf2-dependent antioxidant response and protects against As(III)-induced lung inflammation *in vitro* and *in vivo*. *Antioxid Redox Signal* 2013;**19**:1647–61.
28. Yan SH, Zhao NW, Geng ZR, Shen JY, Liu FM, Yan D, et al. Modulations of Keap1–Nrf2 signaling axis by TIIA ameliorated the oxidative stress-induced myocardial apoptosis. *Free Radical Bio Med* 2018;**115**:191–201.
29. Toldo S, Marchetti C, Mauro AG, Chojnacki J, Mezzaroma E, Carbone S, et al. Inhibition of the NLRP3 inflammasome limits the inflammatory injury following myocardial ischemia–reperfusion in the mouse. *Int J Cardiol* 2016;**209**:215–20.
30. Xin P, Zhu W, Li J, Ma S, Wang L, Liu M, et al. Combined local ischemic postconditioning and remote perconditioning recapitulate cardioprotective effects of local ischemic preconditioning. *Am J Physiol* 2010;**298**:H1819–31.
31. Nickel AG, von Hardenberg A, Hohl M, Loffler JR, Kohlhaas M, Becker J, et al. Reversal of mitochondrial transhydrogenase causes oxidative stress in heart failure. *Cell Metabol* 2015;**22**:472–84.
32. Gibb AA, Epstein PN, Uchida S, Zheng Y, McNally LA, Obal D, et al. Exercise-induced changes in glucose metabolism promote physiological cardiac growth. *Circulation* 2017;**136**:2144–57.

33. Woo AY, Cheng CH, Waye MM. Baicalein protects rat cardiomyocytes from hypoxia/reoxygenation damage *via* a prooxidant mechanism. *Cardiovasc Res* 2005;**65**:244−53.
34. Bish LT, Morine K, Sleeper MM, Sanmiguel J, Wu D, Gao GP, et al. Adeno-associated virus (AAV) serotype 9 provides global cardiac gene transfer superior to AAV1, AAV6, AAV7, and AAV8 in the mouse and rat. *Hum Gene Ther* 2008;**19**:1359−68.
35. Hausenloy DJ, Yellon DM. Targeting myocardial reperfusion injury—the search continues. *N Engl J Med* 2015;**373**:1073−5.
36. Hausenloy DJ, Yellon DM. Myocardial ischemia−reperfusion injury: A neglected therapeutic target. *J Clin Invest* 2013;**123**:92−100.
37. Cao S, Chao D, Zhou H, Balboni G, Xia Y. A novel mechanism for cytoprotection against hypoxic injury: δ-Opioid receptor-mediated increase in Nrf2 translocation. *Br J Pharmacol* 2015;**172**:1869−81.
38. Ashrafian H, Czibik G, Bellahcene M, Aksentijevic D, Smith AC, Mitchell SJ, et al. Fumarate is cardioprotective *via* activation of the Nrf2 antioxidant pathway. *Cell Metabol* 2012;**15**:361−71.
39. de Zeeuw D, Akizawa T, Audhya P, Bakris GL, Chin M, Christ-Schmidt H, et al. Bardoxolone methyl in type 2 diabetes and stage 4 chronic kidney disease. *N Engl J Med* 2013;**369**:2492−503.
40. Ren J, Fu L, Nile SH, Zhang J, Kai G. *Salvia miltiorrhiza* in treating cardiovascular diseases: A review on its pharmacological and clinical applications. *Front Pharmacol* 2019;**10**:753.
41. Wang BQ. *Salvia miltiorrhiza*: Chemical and pharmacological review of a medicinal plant. *J Med Plants Res* 2010;**4**:2813−20.
42. Chouchani ET, Pell VR, Gaude E, Aksentijevic D, Sundier SY, Robb EL, et al. Ischaemic accumulation of succinate controls reperfusion injury through mitochondrial ROS. *Nature* 2014;**515**:431−5.
43. Strom J, Chen QM. Loss of Nrf2 promotes rapid progression to heart failure following myocardial infarction. *Toxicol Appl Pharmacol* 2017;**327**:52−8.
44. Weber NC, Toma O, Wolter JI, Obal D, Mullenheim J, Preckel B, et al. The noble gas xenon induces pharmacological preconditioning in the rat heart *in vivo via* induction of PKC-ε and p38 MAPK. *Br J Pharmacol* 2005;**144**:123−32.
45. Ping PP, Zhang J, Qiu YM, Tang XL, Manchikalapudi S, Cao XN, et al. Ischemic preconditioning induces selective translocation of protein kinase C isoforms epsilon and eta in the heart of conscious rabbits without subcellular redistribution of total protein kinase C activity. *Circ Res* 1997;**81**:404−14.
46. Konishi H, Yamauchi E, Taniguchi H, Yamamoto T, Matsuzaki H, Takemura Y, et al. Phosphorylation sites of protein kinase C δ in H_2O_2-treated cells and its activation by tyrosine kinase *in vitro*. *Proc Natl Acad Sci U S A* 2001;**98**:6587−92.
47. Fujii T, Garcia-Bermejo ML, Bernabo JL, Caamano J, Ohba M, Kuroki T, et al. Involvement of protein kinase C delta (PKC δ) in phorbol ester-induced apoptosis in LNCaP prostate cancer cells—lack of proteolytic cleavage of PKCδ. *J Biol Chem* 2000;**275**:7574−82.
48. Welman A, Griffiths JR, Whetton AD, Dive C. Protein kinase C δ is phosphorylated on five novel Ser/Thr sites following inducible overexpression in human colorectal cancer cells. *Protein Sci* 2007;**16**:2711−5.
49. Rong H, Liang Y, Niu Y. Rosmarinic acid attenuates β-amyloid-induced oxidative stress *via* Akt/GSK-3β/Fyn-mediated Nrf2 activation in PC12 cells. *Free Radical Bio Med* 2018;**120**:114−23.
50. Xin Y, Bai Y, Jiang X, Zhou SS, Wang YH, Wintergerst KA, et al. Sulforaphane prevents angiotensin II-induced cardiomyopathy by activation of Nrf2 *via* stimulating the Akt/GSK-3ss/Fyn pathway. *Redox Biol* 2018;**15**:405−17.
51. Sarbassov DD, Guertin DA, Ali SM, Sabatini DM. Phosphorylation and regulation of Akt/PKB by the rictor-mTOR complex. *Science* 2005;**307**:1098−101.
52. Feng H, Hu L, Zhu H, Tao L, Wu L, Zhao Q, et al. Repurposing antimycotic ciclopirox olamine as a promising anti-ischemic stroke agent. *Acta Pharm Sin B* 2020;**10**:434−46.
53. Case N, Thomas J, Sen B, Styner M, Xie ZH, Galior K, et al. Mechanical regulation of glycogen synthase kinase 3β (GSK3 β) in mesenchymal stem cells is dependent on Akt protein serine 473 phosphorylation *via* mTORC2 protein. *J Biol Chem* 2011;**286**:39450−6.
54. Takahashi-Yanaga F, Taba Y, Miwa Y, Kubohara Y, Watanabe Y, Hirata M, et al. Dictyostelium differentiation-inducing factor-3 activates glycogen synthase kinase-3β and degrades cyclin D1 in mammalian cells. *J Biol Chem* 2003;**278**:9663−70.
55. Doornbos RP, Theelen M, van der Hoeven PCJ, van Blitterswijk WJ, Verkleij AJ, Henegouwen PMPVE. Protein kinase C zeta is a negative regulator of protein kinase B activity. *J Biol Chem* 1999;**274**:8589−96.
56. Lu DM, Huang J, Basu A. Protein kinase C epsilon activates protein kinase B/Akt *via* DNA-PK to protect against tumor necrosis factor-α-induced cell death. *J Biol Chem* 2006;**281**:22799−807.
57. Best SA, De Souza DP, Kersbergen A, Policheni AN, Dayalan S, Tull D, et al. Synergy between the KEAP1/NRF2 and PI3K pathways drives non-small-cell lung cancer with an altered immune microenvironment. *Cell Metabol* 2018;**27**:935−943 e4.
58. Mitsuishi Y, Taguchi K, Kawatani Y, Shibata T, Nukiwa T, Aburatani H, et al. Nrf2 redirects glucose and glutamine into anabolic pathways in metabolic reprogramming. *Canc Cell* 2012;**22**:66−79.